A COMPARISON OF SMALL FIELD OUTPUT FACTORS FOR STEREOTACTIC RADIATION THERAPY

A Dissertation
Presented to
The Academic Faculty

by

Michael Justice

In Partial Fulfillment
of the Requirements for the Degree
Master's in Medical Physics in the
George W. Woodruff School of Mechanical Engineering

Georgia Institute of Technology
December 2024

A COMPARISON OF SMALL FIELD OUTPUT FACTORS FOR STEREOTACTIC RADIATION THERAPY

Approved by:

Dr. Chris Wang [Advisor]
School of Mechanical Engineering
Georgia Institute of Technology

Dr. Eric Elder
School of Mechanical Engineering
Georgia Institute of Technology

Mr. Kayhan Mohajeri
Chief Medical Physicist
Morton Plant Hospital - BayCare

Date Approved: April 03, 2024

[To all the lives impacted by the battle against cancer]

ACKNOWLEDGEMENTS

I would like to offer a special thanks to Kayhan Mohajeri for all of his support and guidance. His belief in me has changed the course of my life, and I will forever be grateful.

TABLE OF CONTENTS

ACKNOWLEDGEMENTS **iv**

LIST OF TABLES **vii**

LIST OF FIGURES **viii**

LIST OF SYMBOLS AND ABBREVIATIONS **x**

SUMMARY **xi**

CHAPTER 1. Introduction **1**
1.1 Background **1**
1.2 Problem Statement **4**
1.3 Research Objectives **5**
1.4 Significance of the Study **6**
1.5 Scopes and Limitations **7**
1.5.1 Scope: 7
1.5.2 Limitations: 7
1.6 Methodology Overview **8**
1.7 Thesis Structure **9**

CHAPTER 2. Literature review **10**
2.1 The Varian Edge **10**
2.2 Treatment Planning Systems (TPS) **11**
2.3 Dose Calculation Algorithm **12**
2.4 Small-Field Output Factors **13**

CHAPTER 3. Methodology **15**
3.1 Literature Review and Data Preparation **15**
3.2 Eclipse Setup and Plan Generation **21**
3.3 Instrumentation Setup and Calibration **23**
3.4 Data Acquisition **23**
3.5 Data Analysis **24**

CHAPTER 4. Results **26**
4.1 Measured Output Factors **26**

CHAPTER 5. Discussion **29**
5.1 Interpretation of Results **29**
5.1.1 Jaw Measurements 29
5.2 Clinical Impact and Relevance **35**
5.3 Limitations of the Study **41**
5.4 Suggestions for Future Research **41**

CHAPTER 6. Conclusion **44**

6.1 Summary of Findings 44

APPENDIX A. OPF Measurements 45
A.1 Jaw-Only OPFs 45
A.2 MLC OPFs 50

APPENDIX B. Retrospective Analysis data 55
B.1 Clear Checks 55
B.2 SRS MapCheck QA 64

APPENDIX C. Python Code 81

REFERENCES 82

LIST OF TABLES

Table 3-1: Equivalent Squares (cm) 16
Table 3-2: Extended Output Factors for Measurements using the Exradin A16 Micro ion chamber 18
Table 3-3: Extended Output Factors for Measurements using the Sun Nuclear EDGE diode detector 19
Table 3-4: Extended Output Factors for Measurements using the IBA Razor diode detector 20
Table 4-1: Cumulative Percentage Differences (%) when Comparing Measured and Literature OPFs by Field Size, Jaws Only 27
Table 4-2: Cumulative Percentage Differences (%) when Comparing Measured and Eclipse OPFs by Field Size, MLC Shaped Fields 28
Table A-1: OPF Measurements using Exradin A16 Micro Ion Chamber (Jaws) 46
Table A-2: OPF Measurements using Sun Nuclear EDGE Diode Detector (Jaws) 47
Table A-3: OPF Measurements using IBA Razor Diode Detector (Jaws) 48
Table A-4: Cumulative OPF Measurementts (Jaws) 49
Table A-5: OPF Measurements using Exradin A16 Micro Ion Chamber (MLCs) 51
Table A-6: OPF Measurements Using Sun Nuclear EDGE Diode Detector (MLCs) 52
Table A-7: OPF Measurements using IBA Razor Diode Detector (MLCs) 53
Table A-8: Cumulative OPF Measurementts (MLCs) 54

LIST OF FIGURES

Figure 3-1: Literature provided output correction factors for all three detectors used.[1,13] 16
Figure 3-2: Spline interpolation of output correction factors for Exradin A16 Micro ion chamber 18
Figure 3-3: Spline interpolation of output correction factors for Sun Nuclear EDGE diode detector 19
Figure 3-4: Spline interpolation of output correction factors for IBA Razor diode detector 20
Figure 3-5: Screenshot of OPFs inserted into beam configuration, using the AXBe data 21
Figure 3-6: Screenshot of Eclipse planning 22
Figure 3-7: Example of 10x10cm MLC field, showing jaw position 0.5cm retracted from MLCs in all directions 22
Figure 4-1: Formatting rules used for percentage difference measurements 26
Figure 5-1: Measured OPFs for several detectors on the Cyberknife 6MV, cone-based delivery, according to Sun Nuclear 30
Figure 5-2: Comparison of the average measured OPF with error bars of 1 standard deviation, by field size, compared to the AXBe literature values 33
Figure 5-3: Comparison of the average measured OPF with error bars of 1 standard deviation, by field size, compared to the Eclipse measured values 34
Figure 5-4: Clear Check for case 98706 37
Figure 5-5: SRS-MapCheck QA for case 98706 original plan 39
Figure B-1: Clear Check Case 13100 56
Figure B-2: Clear Check case 13125 57
Figure B-3: Clear Check case 41080 58
Figure B-4: Clear Check case 17656 59
Figure B-5: Clear Check case 88942 60
Figure B-6: Clear Check case 38946 61
Figure B-7: Clear Check case 59758 62
Figure B-8: Clear Check case 20063 63
Figure B-9: SRS Mapcheck QA case 13100 original plan 65
Figure B-10: SRS Mapcheck QA case 13100 AXBe plan 66
Figure B-11: SRS Mapcheck QA case 13125 original plan 67
Figure B-12: SRS Mapcheck QA case 13125 AXBe plan 68
Figure B-13: SRS Mapcheck QA case 41080 original plan 69
Figure B-14: SRS Mapcheck QA case 41080 AXBe plan 70
Figure B-15: SRS Mapcheck QA case 17656 original plan 71
Figure B-16: SRS Mapcheck QA case 17656 AXBe plan 72
Figure B-17: SRS Mapcheck QA case 88942 original plan 73
Figure B-18: SRS Mapcheck QA case 88942 AXBe plan 74
Figure B-19: SRS Mapcheck QA case 38946 original plan 75
Figure B-20: SRS Mapcheck QA case 38946 AXBe plan 76
Figure B-21: SRS Mapcheck QA case 59758 original plan 77
Figure B-22: SRS Mapcheck QA case 59758 AXBe plan 78

Figure B-23: SRS Mapcheck QA case 20063 original plan 79
Figure B-24: SRS Mapcheck QA case 20063 AXBe plan 80

LIST OF SYMBOLS AND ABBREVIATIONS

AXB	AcurosXB 15.6
AXBe	AcurosXB 15.6 with extended output factor table
BP^2	IBA Blue Phantom2 Tank
FFF	Flattening filter free
FSRT	Fractionated stereotactic radiotherapy
LBTE	Linear Boltzmann transport equation
LCPE	Lateral charged particle equilibrium
MC	Monte-Carlo
MLC	Multi-leaf collimator
MV	Megavoltage
OCF	Output correction factor
OPF	Output factor
SBRT	Stereotactic body radiotherapy
SRS	Stereotactic radiosurgery
SRT	Stereotactic radiotherapy
TPS	Treatment planning system

SUMMARY

This study investigates the clinical application of newly published small-field output factors (OPFs) for the AcurosXB 15.6 (AXB) algorithm in Varian's Eclipse treatment planning system (TPS). The primary goal is to validate the extended AXB (AXBe) model's accuracy in calculating dose for small-field geometries, which are known to be challenging for conventional dosimetry. Measurements were conducted using the Exradin A16 Micro ion chamber, the Sun Nuclear EDGE diode, and the IBA Razor diode to evaluate the capacity of these detectors to reliably capture small field OPFs for jaw-defined and MLC-defined fields.

This thesis offers a comprehensive comparison between measured OPFs, values provided by existing literature, and the OPFs predicted by Eclipse TPS when implementing the AXBe algorithm, identifying trends and discrepancies across detectors and field sizes. Findings from this study affirm the AXBe model's reliability while offering insight into the performance of each detector. The discussion evaluates the clinical relevance of the AXBe model, potential limitations of the methodology used, and suggestions for further research. Future recommendations include expanding this study to include different beam energies, testing additional detectors, and considering long-term clinical trials to further validate the AXBe model for use in stereotactic radiotherapy planning.

CHAPTER 1. INTRODUCTION

1.1 Background

Clinical radiation therapy (or radiotherapy) is a relatively recent advancement in modern medicine. It involves the use of targeted radiation to alter cells on a molecular level, typically using high-energy x-rays in the megavoltage range, produced by linear accelerators. These accelerators are designed to deliver radiation accurately to a target by using various beam-shaping and intensity modulation techniques to control both the shape and distribution of the beam. The primary goal of radiotherapy is to produce ionizations in the DNA of targeted cells, leading to eventual cell death. This process is widely used in the treatment of malignant cancers and has applications in treating benign conditions, such as keloids, neurological disorders, and vascular malformations.

Radiotherapy has quickly become a cornerstone in the treatment regimen for many types of cancer and is often used alongside other treatment modalities such as chemotherapy, surgery, and immunotherapy. Despite its increasing use, radiotherapy remains a field fraught with uncertainties. Many challenges associated with radiotherapy arise from the difficulty in observing radiation in real time within a clinical setting and the stochastic nature of radiation interactions at the cellular level. These uncertainties require allowances for deviations between the planned and delivered doses. As a result, complex radiation plans are often analyzed prior to patient delivery to ensure any variances are within an acceptable limit, with the understanding that the actual dose distribution may differ from what was initially planned.

One critical parameter in treatment planning and verification is the output factor (OPF) applied to the linear accelerator. The OPF is a scatter correction factor that varies depending on factors such as field size, beam energy, and the specific treatment setup or machine conditions under which it is measured. It is defined as the ratio of the absorbed dose to water at a given point for a specific clinical field to the absorbed dose at the same point for a reference field, typically a 10 cm × 10 cm field.[1] According to TRS-483, the output factor **Ω** can be expressed using the formula:

$$\Omega_{Q_{clin},Q}^{f_{clin},f_{ref}} \qquad \text{Eq. 1}$$

where f_{clin} and f_{ref} refer to the clinical non-reference field and the conventional reference field, respectively, and Q_{clin} and Q represent the beam qualities of these fields. While TRS-483 provides the standard definition, the OPF can also be described using f_{max} and Q_{max}, comparing the clinical field to the maximum field size on the machine instead of the 10 cm × 10 cm reference field.

Each linear accelerator undergoes a detailed calibration process during commissioning, which includes verifying the OPFs for all beam energies to published reference data. To ensure accurate treatment planning and dose measurement, clinical sites are equipped with planning software and dose calculation models. The algorithms utilized by these models must consider factors such as tissue heterogeneity, energy dependence, and irregular field shapes. Among these models, the Monte Carlo model is widely regarded as the most accurate in predicting particle behavior due to its detailed simulation of radiation interactions.[2] However, its computational complexity also makes it impractical in clinical settings where expediency is often a concern. The AcurosXB (AXB) advanced dose

calculation model offers a balance between accuracy and computational speed, solving the Linear Boltzmann transport equation to predict radiation behavior accurately and efficiently.[3,4] This study focuses on evaluating the Varian Edge linear accelerator at Morton Plant Hospital (Edge), using the Eclipse planning software and AXB beam models.

Advancements in planning software, beam modeling, and accelerator capabilities have allowed for the delivery of more complex radiation treatments. Given these improvements, the use of high-dose small-field treatments, generically called stereotactic radiotherapy (SRT), has become routine in radiation therapy with up to 77% of clinics reporting at least some involvement with their use.[5] SRT treatments can be further classified as a single intracranial treatment (stereotactic radiosurgery or SRS), fractionated intracranial treatment (fractionated stereotactic radiotherapy or FSRT) and fractionated extracranial treatment (stereotactic body radiotherapy or SBRT).[5] These treatment types require small, clearly defined target volumes, tight dose margins, high fractional doses, and are usually delivered in 1-5 fractions. Historically, these treatments were difficult to design, plan, and accurately deliver. The combination of AXB with modern imaging has drastically helped with the planning of these treatments. Furthermore, the Varian Edge is equipped with a high-definition multi-leaf collimator to aid in the delivery of small-field radiation, as well as the HyperArc planning software to streamline and expedite the planning and delivery process. These advancements have greatly reduced the time it takes to plan and deliver SRT treatments, as well as increasing confidence in their accuracy. Regardless, SRT still faces unique challenges. The Radiological Physics Center (RPC) presented a 23 center-wide study, including nearly 100 linear accelerators, showing nearly a 5% difference between the RPC-measured and self-reported measured OPFs for small fields.[6]

Furthermore, the RPC noted that the planning software often over-estimated the output for small fields.[6] Due to the uncertainties in small-field OPFs and the inherently small field sizes utilized for SRT planning, accurate beam modeling remains a challenge. As will be discussed, as field sizes become considerably small, beam modeling becomes increasingly complex and less reliable.

1.2 Problem Statement

Equation 1 shows that once the output for a given energy of radiation for a 10x10 cm field has been determined, OPFs can be determined for other non-reference fields of the same energy. There are instances, however, where the relationship between the non-reference field and the reference 10cm field does not produce accurate OPFs. Examples for when this happens would be for significantly irregular or small fields.[1,6] For this study, the focus will be on the effects small fields have on output factors.

TRS-483 defines small fields as having three important physical characteristics:

i. There is a loss of lateral charged particle equilibrium (LCPE) on the beam axis;
ii. There is partial occlusion of the primary photon source by the collimating devices on the beam axis;
iii. The size of the detector is similar or large compared to the beam dimensions.

The current AXB model used in this study provides OPFs for fields as small as 3x3 cm. According to a Varian representative, A. Little, the AXB model for OPFs can be split into three factors: phantom scatter, head scatter, and collimator backscatter.[12] He stated that for

small fields, the model correctly calculates the phantom and head scatter but uses the collimator backscatter factor of only the smallest field available. While the contribution of this scatter is likely very small in comparison, this means that the current model is likely to overestimate the OPF for fields smaller than 3x3cm. Recently, the *Journal of Applied Medical Physics* made a publication containing an extended AcurosXB output factor model (AXBe), which includes values for fields as small as 1x1 cm.[9] In retrospective analyses of SRT treatments performed on the Edge, areas of lower-than-expected dose (cold spots) were observed, presumably due to inaccuracies in calculating the OPF for the small fields being used. This study aims to analyze the new AXBe model, compare the dose distribution between plans created by the AXB and AXBe, and to determine if the collected data on this accelerator matches that of published data. Ideally, this study will verify whether the AXBe model for small-field OPFs improves the accuracy of SRT dose distributions.

1.3 Research Objectives

The primary objective of this research is to evaluate the accuracy of OPFs for small fields using the AXBe model, with the aim of improving dose distribution for SRT on the Varian Edge linear accelerator. To achieve this goal, the study will address several specific objectives:

i. Expand the Output Factor Model: Utilize the AXBe model to generate OPF values for fields as small as 1x1 cm, improving upon the 3x3 cm field size minimum currently established with the AXB model.

ii. Verify Beam Model Effectiveness: Measure OPFs for fields as small as 1x1 cm to compare to the Eclipse calculated OPFs to assess the accuracy of the AXBe model's capabilities.

iii. Cross-Reference Data: Compare collected data using various detectors with the current published data to ensure consistency and accuracy.

iv. Address Small-Field Complications: Collect field size data using jaw-defined fields described in the published data, as well as with MLC-defined fields to explore and address the complications associated with SRT delivery.

v. Retrospective Analysis: Compare a variety of delivered SRT plans using both the AXB and AXBe models to reinforce the validity of the AXBe beam model.

1.4 Significance of the Study

The Varian Edge is a specialized version of the Varian TrueBeam linear accelerator, specifically designed for SRT treatments. Commissioned in 2020, the Edge has since played a critical role in delivering high-precision radiation therapy, particularly for patients requiring SRT. Due to the high volume of SRT treatments performed on this machine, accurate dose distribution for small fields is a significant concern.

Inaccuracies in small-field OPFs are a well-recognized issue within the field of medical physics. While this study does not aim to introduce novel solutions to this problem, its significance lies in the clinical application of the newly developed AXBe model, as well as the feasibility by which a clinical physicist may implement and validate such a model. By integrating this model into current treatment protocols, this research seeks to enhance

the accuracy of dose distribution for small fields, thereby ensuring that patients receive the most precise and effective treatments possible.

Looking ahead, there are plans to establish a trigeminal neuralgia treatment program utilizing small-sized cones on the Edge. This research could also provide a framework for data collection and analysis that would support the development of such a program. In doing so, this study not only addresses immediate clinical needs but also contributes to the future advancement of specialized treatment options on the Edge.

1.5 Scopes and Limitations

1.5.1 Scope:

This study will focus on evaluating the effectiveness of the AXB and AXBe dose calculation models specifically for the Varian Edge linear accelerator. The research is designed to apply only to the clinical settings involving this particular machine. While the findings may have implications for other treatment machines or dose calculation models, the scope of this study is confined to the Edge and the data collected from its use. The retrospective data analyzed will also be restricted to SRT treatments delivered exclusively on this machine.

1.5.2 Limitations:

The AXBe model provides OPF values for field sizes down to 1x1 cm. While SRT plans may use fields smaller than 1x1 cm, measurements will be confined to a minimum field size of 1 cm. This constraint may limit the study's ability to fully assess the model's accuracy for very small fields.

Furthermore, this study will incorporate measurements from fields defined with jaw-only and MLC methods. The Varian Edge's ability to treat multiple lesions simultaneously necessitates the use of complex MLC motion. While the primary goal is to measure and enhance OPF calculations for single small fields, the inclusion of data with and without MLCs aims to provide insights into potential challenges associated with SRT treatments. However, the field arrangement for MLCs during SRT delivery is significantly more complex than the MLC fields measured in this study, and exploration of these complex scenarios is not the primary focus of this research.

1.6 Methodology Overview

The methodology for this study centers on expanding and verifying the OPF table in Eclipse using the AXBe algorithm. Data was collected using the Exradin A16 Micro ion chamber, Sun Nuclear EDGE diode, and IBA Razor diode. These detectors were selected for their compatibility with small-field measurements and the availability of published output correction factors (OCFs). Literature-derived OCFs were interpolated using a spline technique to address missing field sizes, allowing for continuous correction factors across the measurement range.

Measurements were taken using the IBA Blue Phantom^2 water tank. Each detector was set up according to established protocols, then repeat detector readings were taken and recorded for various field sizes. The study involved both jaw-defined fields and multi-leaf collimator (MLC) fields, each planned on a 50x50 cm virtual phantom.

Data was analyzed by calculating OPFs and comparing them with the literature and Eclipse-generated values. Consistency was assessed through percentage difference

calculations, and standard deviation errors were calculated to gauge variability among the detectors. This rigorous process ensured the reliability of the measured OPFs and their alignment with both literature standards and treatment planning software predictions.

1.7 Thesis Structure

This thesis is organized into six main chapters. Chapter 1 introduces the study, outlining the background, research objectives, and the significance of examining expanded output factors for small-field applications. Chapter 2 reviews the literature, focusing on the treatment machine, treatment planning system, and relevant dose calculation algorithms, establishing the foundation for this study.

Chapter 3 explains the methodology, detailing the selection and calibration of detectors, the setup of experimental conditions, and the computational methods used to interpolate OCFs. Chapter 4 presents data collection and analysis of the results, comparing measured OPFs across multiple detectors with published data to validate Eclipse's OPF calculations for clinical application. Chapter 5 interprets the findings within the context of existing literature, discussing implications for clinical practice, prospective use, and retrospective data analysis.

Chapter 6 summarizes the study’s findings, presenting final insights and recommendations for future research. Finally, the appendices contain supporting documents, including complete OPF data, retrospective analysis data, and the Python code used for data interpolation.

CHAPTER 2. LITERATURE REVIEW

To maintain the scope of this study, it is important to elaborate on important key topics, while still assuming the reader has some basic understanding of radiation therapy.

2.1 The Varian Edge

The Varian Edge is a linear accelerator equipped with advancements specifically designed for small-field radiation therapy. All data collection for this study will be performed on an Edge (serial number 4395), commissioned in 2020. This machine provides many tools to aid in the delivery of SRT, such as a patient support assembly with 6 degrees of movement, various types of patient imaging, and enhanced motion detection, among others.[11] While these factors aid in the delivery of SRT, the scope of this study will not be focusing on how these factors affect the accurate delivery of radiation. This study will be aimed only at analysing the calculations of OPFs for small fields to determine dose distribution. Therefore, the key characteristics of this machine that will be addressed are the multileaf collimator, the dynamic jaws, and the photon energies available.

The Edge comes equipped with an HD120^{TM} Multileaf collimator (HD MLC), with each leaf near the centre of the field being 2.5mm in diameter. Additionally, the jaws in the collimator have dynamic tracking, allowing them to conform to the smallest size possible, reducing intraleaf leakage.[11] During single, small lesions, the dynamic jaws can shape tightly to the MLC field, minimizing radiation contribution from this leakage. For multi-lesion treatments, the separation between these lesions may lead to a significant increase

in the jaw field size. This study will analyse data collected using only secondary jaw collimation, as well as MLC collimation in conjunction with dynamic jaw tracking.

For this study, another concern to address will be the photon energies available. Varian products may have a variety of available energies in both standard megavoltage with flattening filter (MV), and megavoltage flattening filter free (FFF). The Edge being used has four available photon energies: 6MV, 10MV, 6FFF, and 10FFF. This study will only focus on the 6FFF energy, as all SRS plans on this machine use 6FFF.

Of note, the Edge also utilizes the HyperArc planning software for SRT treatments of the brain (FSRT and SRS). All retrospective SRT treatments in this study were performed using HyperArc. Therefore, all comparison plans created using the new AXBe model will be created using the same software.

2.2 Treatment Planning Systems (TPS)

The treatment planning system (TPS) used for treatment planning on the Edge is the Eclipse v16.1 provided by Varian. The TPS is a platform designed to aid in the creation of radiation treatment plans. Eclipse is the standard planning software for the Edge, as both products are created by Varian. Eclipse is specifically designed to integrate with Aria and other Varian products, allowing for an efficient and streamlined clinical process. Eclipse is equipped with many features to enhance treatment planning, such as the previously mentioned HyperArc software, specially designed for SRS and FSRT planning. The HyperArc software provides features such as tissue objectives, collimator optimization, and increased calculation speeds to improve the treatment planning and delivery process.[11] This combination of software has helped to reduce planning and

treatment times significantly, with current SRT delivery now averaging between 10-15 minutes.[11] During treatment planning, the TPS will reference a dose calculation algorithm to determine the expected dose distribution.

2.3 Dose Calculation Algorithm

Dose calculation algorithms are utilized by the TPS to determine the expected distribution of absorbed dose the patient will receive. Since photon interactions with matter are stochastic as well as dependent on the energy of the incident beam and the density atomic makeup of the tissue it is interacting with, it can be very difficult to accurately determine dose distribution. As previously discussed, the Monte Carlo (MC) method is widely regarded for its superior accuracy among dose calculation algorithms. MC calculations are designed to determine the stochastic interaction of both primary and secondary particles in a medium. By solving the dose distribution of individual particles, this algorithm can be applied to a plan by adjusting for fluence and medium.[11] Due to the complex nature of dealing with stochastic interactions, MC calculations are very time consuming. While the MC algorithm is preferable for accuracy, it is often not clinically practical due to time constraints. For this reason, the TPS can use other models that balance accuracy and expediency. As mentioned, this study will focus on the AcurosXB and extended AcurosXB algorithms.

AXB resolves the long calculation times required by MC by solving for a deterministic variable, rather than the stochastic calculation MC performs. AXB solves for the Linear Boltzmann Transport Equations (LBTEs) for photons and their secondary interactions. LBTEs provide a deterministic value that represents the behavior function for each particle

type. This data can be used in congruence with particle fluence, fluence direction, and applicable stopping powers to determine the dose deposition.[3] This allows AXB to provide dose calculations with reliability comparable to MC, but with greatly reduced calculation times, making it a strong option for clinical use.[4] The current AXB version in use on the Edge is AXB 15.6, with OPFs for field sizes ranging from 40x40cm down to 3x3cm. In 2022, Ning Genevieve Wu published the extended model in the Journal of Applied Clinical Medical Physics.[9] As mentioned, this study will be comparing the AXB model with the AXBe model using the 15.6 version, extending the OPF table to include field sizes as small as 1x1cm.

2.4 Small-Field Output Factors

As mentioned above, small fields are defined with three major characteristics: a loss of lateral charged equilibrium, partial occlusion of the primary photon source, and/or the case where the detector is of similar or larger size than the radiation field. The goal for small-field dosimetry is to produce accurate and reliable OPF measurements despite the inconsistencies created by these characteristics. Small-field dosimetry is a problem that has been researched and formalized for several years, with published data providing guidelines for proper detector use. Regardless, these characteristics provide additional complexities to small-field dosimetry.

When performing dose modeling, the algorithms can take advantage of charged particle equilibrium to create an equality between absorbed dose and collisional kerma. Under the conditions of charged particle equilibrium, the number of charged particles of a given energy entering a volume is equal to the number of charged particles of that energy exiting

a volume. As the incident photon energy increases and as field size decreases, the range of the charged particles created in the volume can begin to exceed the maximum size of the volume. This loss of lateral charged particle equilibrium (LCPE) alters the relation between dose and collisional kerma, creating inconsistencies in the dose calculation model. This relationship can be further worsened when including the presence of tissue heterogeneities.[1,4]

The second characteristic of small fields is the partial occlusion of the photon source by the collimating system. In theory, a linear accelerator should provide a point source, however, a volume is often given to the photon source to account for inconsistencies. The primary photon source, or focal spot, can be adjusted in the beam modeling in Eclipse, and in very small fields, partial occlusion may occur, which worsens as the target location moves laterally away from the center of the beam. This can lead to an increase in the relative size of the penumbra for small fields.

Finally, small-field OPFs present challenges due to the physical limitations of available detectors. It is essential to use detectors with active volumes that are appropriately sized for the fields being measured. As technology advances, newer detectors with smaller active volumes are becoming more common, increasing the availability of detectors suitable for small-field measurements. By referencing published data and using appropriate small-field detectors, it is possible to avoid discrepancies between detector volumes and the field sizes being measured.

CHAPTER 3. METHODOLOGY

3.1 Literature Review and Data Preparation

The primary goal of this research is to expand the output factor table for AXB 15.6 in Eclipse to match the extended table presented by Ning Genevieve Wu. The AXBe data was collected using the Standard Imaging Exradin W2-1x1 scintillator detector, known for its precision in measuring small fields without the need for correction factors, as highlighted in TRS-483. However, many clinical physicists may not have a scintillator detector readily available. To address this concern, this research utilized a combination of one ion chamber detector and two diode detectors: the Exradin A16 Micro ion chamber, the Sun Nuclear EDGE diode, and the IBA Razor diode. The selection of these detectors aimed to provide a variety of detector types capable of acquiring small-field measurements while also ensuring that sufficient published OCFs were available for these small fields. To ensure the accuracy of measurements, OCFs were required for each detector. A study published in 2020 by C. Smith, et al., compared measurements of small-field OPFs with and without OCFs, using both square fields and cones for a variety of detectors.[10] The unique characteristics of small fields, as previously presented by TRS-483, tend to cause detector readings to become inaccurate. These changes are dependent on the physical characteristics of each detector and may cause the detector to either over- or under-respond. OCFs are used to make up for these discrepancies, and OPFs measured with the correction factors tended to have improved consistency and accuracy when compared to those measured without correction factors.[10]

		Equivalent Square Field Size sclin (cm)									
		8	6	4	3	2.5	2	1.5	1.2	1	0.8
Detector Type	Exradin A16 Micro	1	1	1	1	1.001	1.003	1.008	1.017	1.027	1.043
	Sun Nuclear Edge	1	1	1	0.999	0.998	0.994	0.986	0.976	0.966	0.951

		Equivalent Square Field Size sclin (cm)								
		10	5	4	3	2	1.5	1	0.8	0.5
Detector Type	IBA Razor Diode	0.999	1.009	1.017	1.026	1.031	1.029	1.007	1.005	0.992

Figure 3-1: Literature provided output correction factors for all three detectors used.[1,13]

As seen in Figure 3-1, OCFs are not provided for all field sizes relevant to the study, and therefore needed to be interpolated. To facilitate this, the following equation can be used to calculate the equivalent square for fields larger than 10 mm:

$$Equivalent\ Square\ (S) = \frac{4A}{P} \qquad \text{Eq. 2}$$

Where A is the area of the field (X-jaw * Y-jaw, in cm) and P is the perimeter of the field (2*(X-jaw + Y-jaw) in cm). This equation was used to calculate equivalent squares for all field sizes introduced in the AXBe model. While it is acceptable to measure the FWHM to determine the field sizes at the time of data collection, this method is both more time consuming and has shown little to no benefit over the equivalent square method.[17]

Table 3-1: Equivalent Squares (cm)

Equivalent Squares												
		Field Size FX(cm)										
		1	2	3	4	5	7	10	15	20	30	40
Field Size FX(cm)	1	1.00	1.33	1.50	1.60	1.67	1.75	1.82	1.88	1.90	1.94	1.95
	2	1.33	2.00	2.40	2.67	2.86	3.11	3.33	3.53	3.64	3.75	3.81
	3	1.50	2.40	3.00	3.43	3.75	4.20	4.62	5.00	5.22	5.45	5.58
	4	1.60	2.67	3.43	4.00	4.44	5.09	5.71	6.32	6.67	7.06	7.27
	5	1.67	2.86	3.75	4.44	5.00	5.83	6.67	7.50	8.00	8.57	8.89
	7	1.75	3.11	4.20	5.09	5.83	7.00	8.24	9.55	10.37	11.35	11.91
	10	1.82	3.33	4.62	5.71	6.67	8.24	10.00	12.00	13.33	15.00	16.00
	15	1.88	3.53	5.00	6.32	7.50	9.55	12.00	15.00	17.14	20.00	21.82
	20	1.90	3.64	5.22	6.67	8.00	10.37	13.33	17.14	20.00	24.00	26.67
	30	1.94	3.75	5.45	7.06	8.57	11.35	15.00	20.00	24.00	30.00	34.29
	40	1.95	3.81	5.58	7.27	8.89	11.91	16.00	21.82	26.67	34.29	40.00

Once the equivalent squares were calculated, OCF literature values were collected for each detector, and a spline interpolation was performed to provide correction factors for each equivalent square.

This spline method was preferred for its ability to create a smooth, piecewise curve, and was implemented in Google Colab using custom Python code (detailed in Appendix A). The code generates interpolated OCFs for equivalent squares ranging from the smallest to largest literature-provided field sizes, in increments of 0.01 cm, facilitating the acquisition of correction factors for all measured fields across the three detectors.

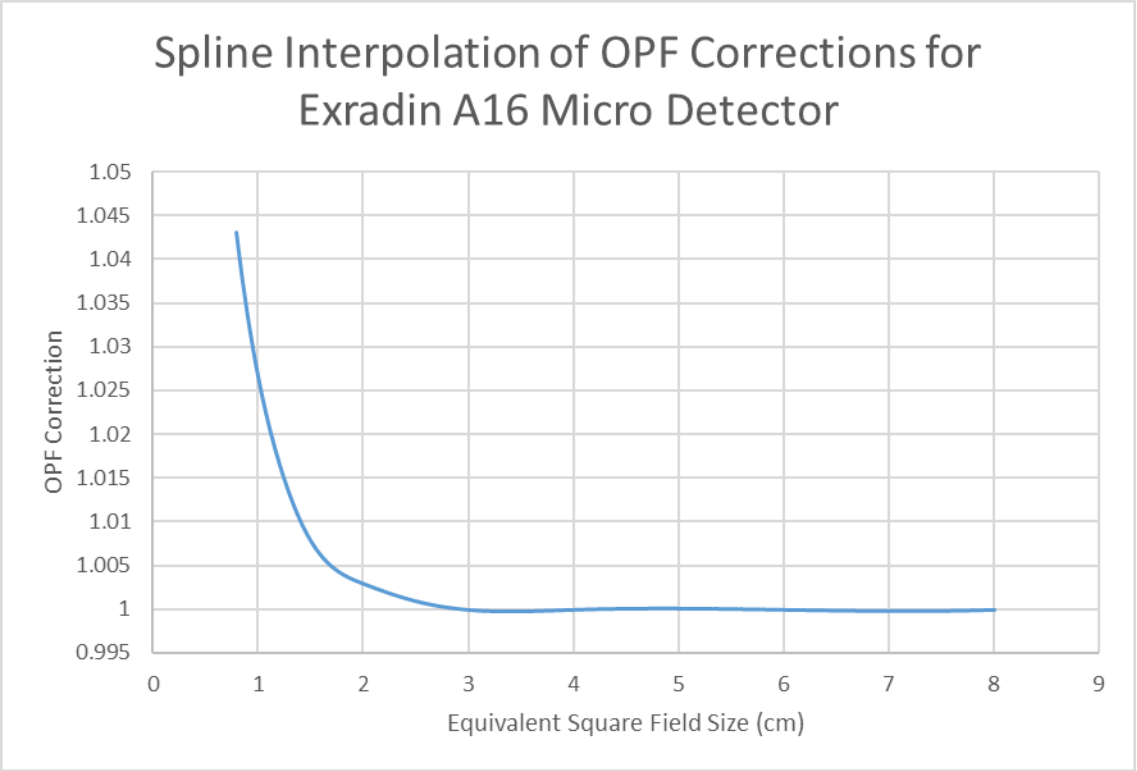

Figure 3-2: Spline interpolation of output correction factors for Exradin A16 Micro ion chamber

Table 3-2: Extended Output Factors for Measurements using the Exradin A16 Micro ion chamber

Expanded Output Factor for Exradin A16 Micro

Field Size FX(cm)	Field Size FX(cm) 1	2	3	4	5	7	10	15	20	30	40
1	1.027	1.012	1.008	1.006	1.005	1.005	1.004	1.004	1.003	1.003	1.003
2	1.012	1.003	1.001	1.001	1.000	1.000	1.000	1.000	1.000	1.000	1.000
3	1.008	1.001	1.000								
4	1.006	1.001									
5	1.005	1.000			1.000						
7	1.005	1.000									
10	1.004	1.000					1.000				
15	1.004	1.000									
20	1.003	1.000									
30	1.003	1.000									
40	1.003	1.000									

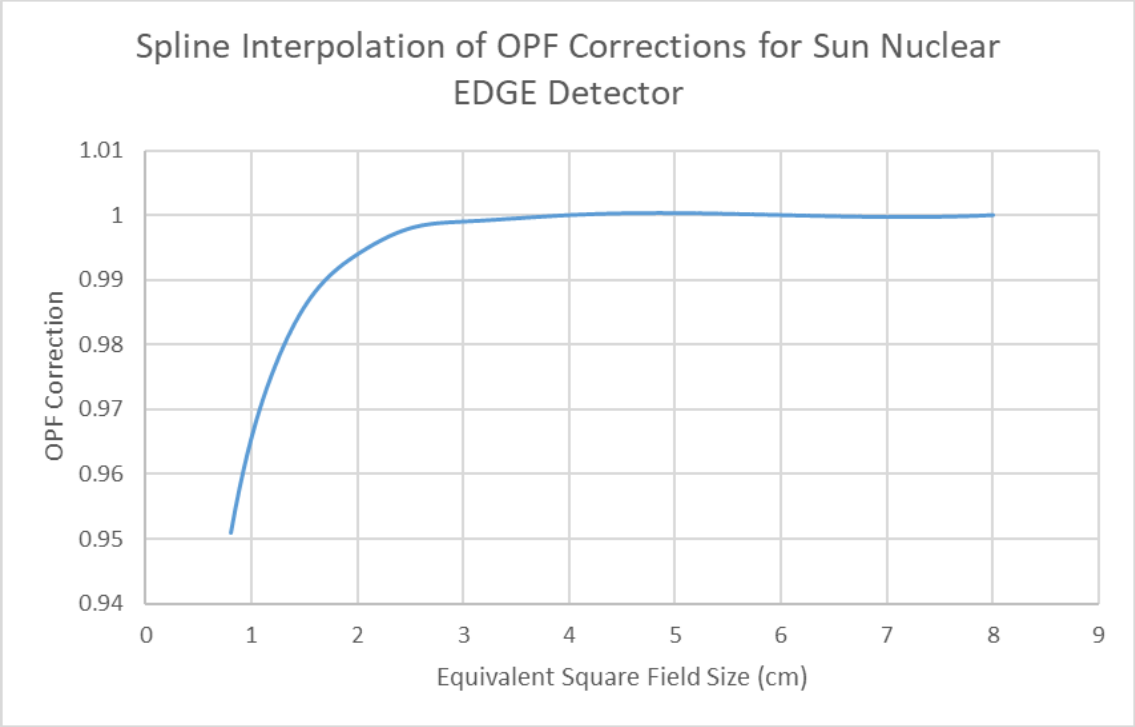

Figure 3-3: Spline interpolation of output correction factors for Sun Nuclear EDGE diode detector

Table 3-3: Extended Output Factors for Measurements using the Sun Nuclear EDGE diode detector

Expanded Output Factor for Sun Nuclear EDGE

Field Size FX(cm)	Field Size FX(cm)	1	2	3	4	5	7	10	15	20	30	40
	1	0.966	0.981	0.986	0.988	0.990	0.991	0.992	0.993	0.993	0.993	0.993
	2	0.981	0.994	0.997	0.999	0.999	0.999	0.999	1.000	1.000	1.000	1.000
	3	0.986	0.997	0.999								
	4	0.988	0.999									
	5	0.990	0.999			1.000						
	7	0.991	0.999									
	10	0.992	0.999					1.000				
	15	0.993	1.000									
	20	0.993	1.000									
	30	0.993	1.000									
	40	0.993	1.000									

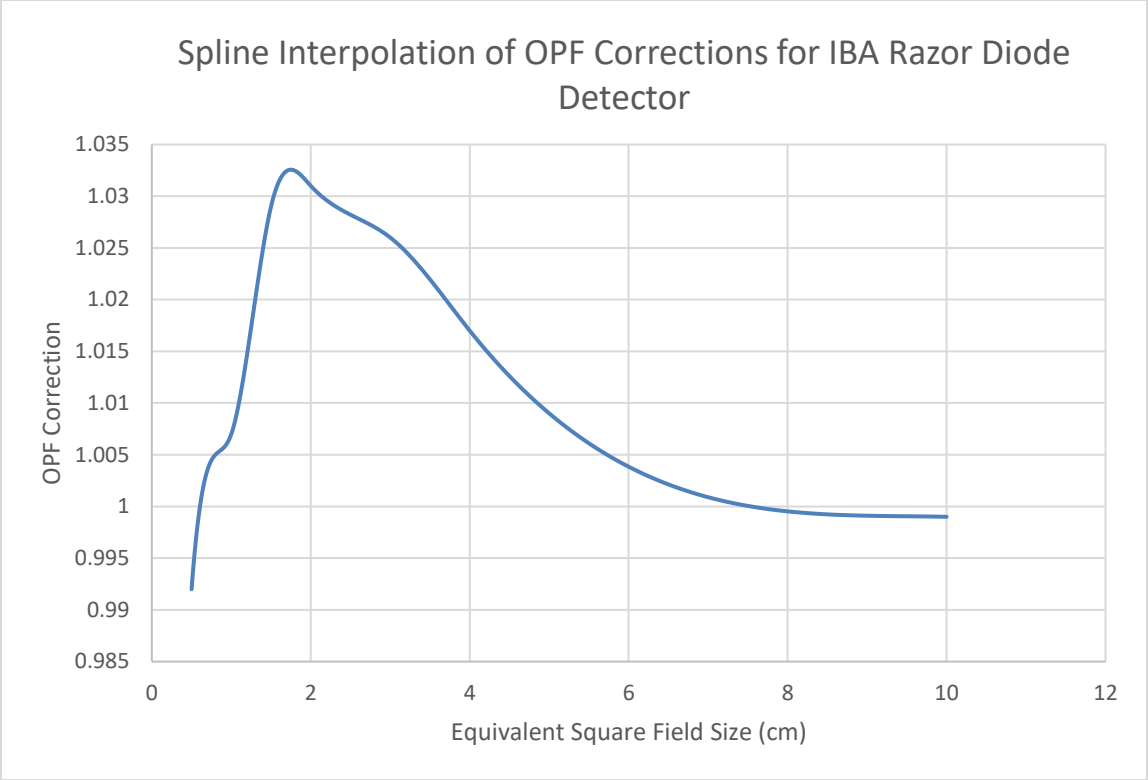

Figure 3-4: Spline interpolation of output correction factors for IBA Razor diode detector

Table 3-4: Extended Output Factors for Measurements using the IBA Razor diode detector

Expanded Output Factor for IBA Razor Diode

Field Size FX(cm)	Field Size FX(cm)											
		1	2	3	4	5	7	10	15	20	30	40
	1	1.007	1.022	1.029	1.031	1.032	1.033	1.032	1.032	1.032	1.032	1.031
	2	1.022	1.031	1.029	1.028	1.027	1.025	1.024	1.022	1.021	1.019	1.019
	3	1.029	1.029	1.026								
	4	1.031	1.028									
	5	1.032	1.027			1.009						
	7	1.033	1.025									
	10	1.032	1.024					1.000				
	15	1.032	1.022									
	20	1.032	1.021									
	30	1.032	1.019									
	40	1.031	1.019									

3.2 Eclipse Setup and Plan Generation

To conduct this research, a beam model was configured utilizing the AXBe published data. Of note, the published data does not have information for a field size of 4cm, however, beam configuration does in fact have this data, as seen from the following screenshot.

	10.0	20.0	30.0	40.0	50.0	70.0	100.0	150.0	200.0	300.0	400.0
10.0	0.739	0.782	0.796	0.799	0.802	0.804	0.807	0.808	0.809	0.809	0.810
20.0	0.794	0.853	0.866	0.873	0.879	0.884	0.888	0.890	0.892	0.893	0.893
30.0	0.804	0.867	0.896	0.907	0.914	0.922	0.928	0.932	0.934	0.937	0.937
40.0	0.807	0.874	0.907	0.921	0.929	0.940	0.947	0.953	0.956	0.958	0.959
50.0	0.810	0.881	0.914	0.930	0.940	0.952	0.962	0.969	0.972	0.975	0.976
70.0	0.814	0.888	0.925	0.943	0.955	0.970	0.982	0.991	0.996	1.000	1.001
100.0	0.816	0.892	0.933	0.953	0.967	0.985	1.000	1.012	1.018	1.024	1.025
150.0	0.818	0.896	0.938	0.960	0.975	0.996	1.013	1.029	1.038	1.046	1.048
200.0	0.819	0.897	0.941	0.963	0.979	1.001	1.020	1.038	1.049	1.058	1.060
300.0	0.821	0.900	0.944	0.967	0.983	1.006	1.028	1.048	1.061	1.072	1.075
400.0	0.822	0.900	0.945	0.968	0.985	1.009	1.031	1.052	1.065	1.078	1.080

Figure 3-5: Screenshot of OPFs inserted into beam configuration, using the AXBe data

Once all other data was transcribed, the beam configuration automatically calculated the 4cm values. The above model was used for all AXBe calculated data. To compare the output factors calculated by Eclipse, fields were planned on a virtual 50x50cm phantom using symmetrical jaws, SRS static technique, 6FFF energy, and 100mus. The reference point was set at a depth of 5cm and an SSD of 95cm. Jaw-defined fields were created for all field sizes introduced by the AXBe model, as well as for the 10x10 reference field.

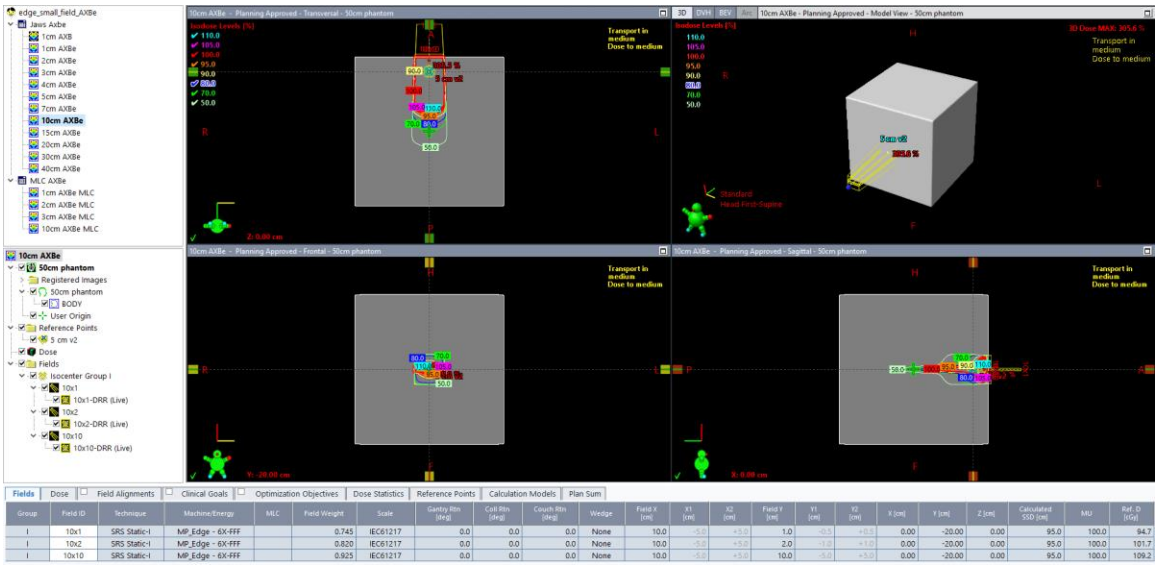

Figure 3-6: Screenshot of Eclipse planning

Afterwards, 9 fields were created using MLCs, ranging from 1x1cm to 3x3 cm, plus an additional 10x10cm. For these plans, the MLCs were set to the measured field size with the jaws set 0.5cm back to simulate dynamic jaw tracking, with all other parameters set the same.

Group	Field ID	Technique	Machine/Energy	MLC
I	10x10	SRS Static-I	MP_Edge - 6X-FFF	Static

Field X [cm]	X1 [cm]	X2 [cm]	Field Y [cm]	Y1 [cm]	Y2 [cm]
11.0	-5.5	+5.5	11.0	-5.5	+5.5

Figure 3-7: Example of 10x10cm MLC field, showing jaw position 0.5cm retracted from MLCs in all directions

Utilizing equation 1, Eclipse OPFs are obtained by dividing the reference dose calculated by Eclipse for each field by the reference dose of the 10x10cm field.

3.3 Instrumentation Setup and Calibration

For data acquisition, the Exradin A16 Micro ion chamber, Sun Nuclear EDGE diode, and IBA Razor diode were used in conjunction with the IBA Blue Phantom2 (BP^2) water tank and a PC electrometer. The tank was carefully set up, leveled, and aligned using the reflection method as described in the BP^2 user manual.[18] The field light was used to align the detectors to the isocenter at the water surface, with a 95 cm SSD, before moving to a depth of 5 cm using the BP^2 software.

Each detector was positioned according to both the BP^2 and individual detector manuals, as well as the recommendations from TRS-483.[1,18] The Razor diode was aligned parallel to the beam, while the Sun Nuclear EDGE diode and Exradin A16 were positioned perpendicular to the beam. Both diodes used 0 voltage bias, while the A16 used a +300V bias. Background readings were recorded prior to all measurements to ensure accurate results. Central axis was determined manually by taking cross-profile measurements in 1mm steps from the initial setup, using a 10x10 cm field.

3.4 Data Acquisition

Data acquisition followed a uniform protocol for all three detectors. After confirming proper alignment, detector depth, and voltage bias according to the previously mentioned setup, background radiation was measured to account for ambient noise. Using the service mode on the Varian Edge, 100 MUs were delivered for each field size, ensuring consistency in beam delivery.

For each field, three separate measurements were recorded using the PC electrometer to ensure repeatability, and any potential outliers were noted. In addition, Eclipse-generated plans for the MLC fields were delivered in treatment mode to confirm jaw and MLC positions. The measurements were repeated under the same conditions to ensure consistency and accuracy across all field sizes.

3.5 Data Analysis

TRS-483 provides a formula for calculating the field OPFs from the detector readings:

$$\Omega_{Q_{clin},Q}^{f_{clin},f_{ref}} = \frac{M_{Q_{clin}}^{f_{clin}}}{M_{Q_{ref}}^{f_{ref}}} * k_{Q_{clin},Q}^{f_{clin},f_{ref}} \quad \text{Eq. 3}$$

Where $M_{Q_{clin}}^{f_{clin}}$ and $M_{Q_{ref}}^{f_{ref}}$ are the detector readings of the measured field and the 10x10cm reference field, respectively, and $k_{Q_{clin},Q}^{f_{clin},f_{ref}}$ or k_q is the output correction factor. Once all three measurements were taken for each field size, the average was taken ($M_{Q_{clin}}^{f_{clin}}$) and divided by the 10x10cm average ($M_{Q_{ref}}^{f_{ref}}$). Using the previously generated spline data, k_q values were obtained for each detector and field size. Using equation 3, the measured OPFs were calculated. For each field size, the average OPF was also calculated across the detectors.

Since the goal of this research is to validate that the clinical data collected matches the published data, a percentage difference calculation was used:

$$Percentage\ difference\ (\%diff) = 100 * \frac{Measured\ Value - Actual\ Value}{Actual\ Value} \quad \text{Eq. 4}$$

Equation 4 was used to compare the measured OPF to the literature OPF, the average measured OPF to the Eclipse calculated OPF, and the Eclipse calculated OPF to the literature OPF. The published data represents fields shaped by the X and Y jaw only, so there was no literature comparison made for MLC fields. Instead, the measured OPFs and average measured OPFs were compared to the Eclipse OPF.

Finally, a standard deviation error was calculated for the averaged OPFs:

$$Error\ (SD) = sqrt\left(\frac{(x_1 - \bar{x})^2 + (x_2 - \bar{x})^2 + (x_3 - \bar{x})^2}{n - 1}\right) \quad \text{Eq. 5}$$

Where X_1, X_2, and X_3 represent OPFs from each detector, $\bar{x}$ is the average OPF, and n is the number of detectors used.

CHAPTER 4. RESULTS

4.1 Measured Output Factors

The OPF data collected was separated into different tables for both jaws-only and MLC measurements, with one table for each detector and one for averages. The percentage difference columns were then given the following conditional formatting:

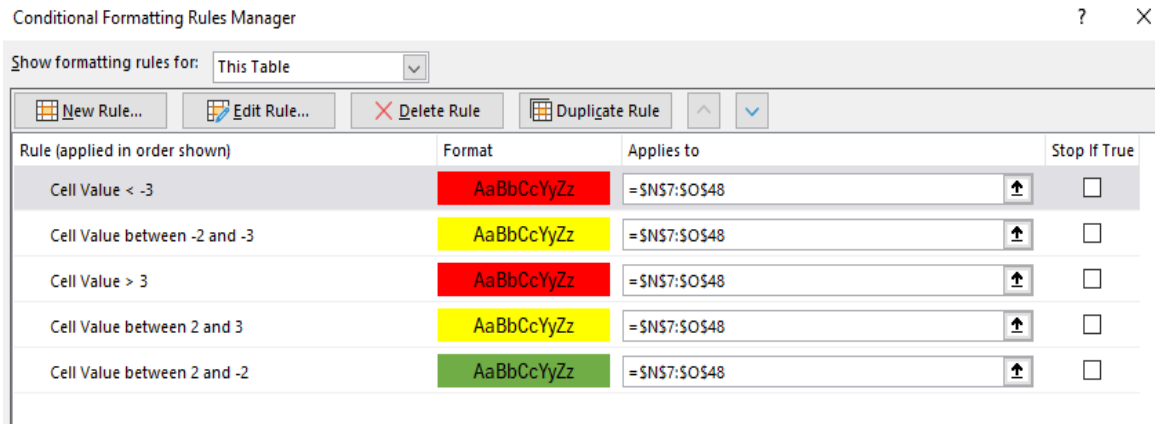

Figure 4-1: Formatting rules used for percentage difference measurements

Where a red value represents a difference of greater than (+/-) 3%, yellow represents a difference between (+/-) 2% and (+/-) 3%, and green represents a difference less than (+/-) 2%.

Ideally, the percentage difference between the measured values and the literature values should be reasonably small. While no specific standards were used, the hope of this study would be to keep percent differences less than 2%, but no more than 3%, as this was the standard requested by the clinical physicists for the machines on which the data was collected.

Table 4-1: Cumulative Percentage Differences (%) when Comparing Measured and Literature OPFs by Field Size, Jaws Only

Average Measured OPF to Literature Percent Differences (%) - Jaws Only				
Field Size (cm)	Exradin A16	Sun Nuclear Edge	IBA Razor	Cumulative
1x1	-2.030	-1.245	-0.666	-1.086
1x2	-0.889	0.569	1.116	0.601
1x3	-1.103	0.992	1.884	0.822
1x4	-1.015	1.376	2.383	1.114
1x5	-1.099	1.549	2.431	1.265
1x7	-0.959	1.638	2.538	1.335
1x10	-0.828	1.866	2.729	1.498
1x15	-0.524	1.994	2.864	1.667
1x20	-0.500	2.057	2.901	1.832
1x30	-0.498	1.984	2.743	1.735
1x40	-0.450	2.002	1.853	1.448
2x1	-3.523	-1.779	0.564	-1.258
2x2	-1.793	-0.253	0.613	-0.221
2x3	-1.408	0.205	0.958	0.165
2x4	-1.107	0.535	1.151	0.249
2x5	-1.171	0.364	0.902	0.268
2x7	-1.051	0.389	1.107	0.319
2x10	-0.617	0.711	1.168	0.555
2x15	-0.306	0.797	1.197	0.660
2x20	0.011	1.008	1.298	0.860
2x30	0.121	0.903	1.417	0.874
2x40	0.292	1.064	1.554	1.031
3x1	-4.641	-2.104	-0.261	-2.029
3x2	-1.809	-0.055	0.876	-0.074
3x3	-2.346	-0.932	-0.117	-0.917
4x1	-4.627	-1.882	-0.057	-2.046
4x2	-1.628	0.277	1.033	0.083
5x1	-4.770	-1.760	-0.002	-1.933
5x2	-1.768	0.170	0.924	0.031
7x1	-4.642	-1.525	0.291	-1.734
7x2	-1.680	0.341	0.859	0.048
10x1	-4.843	-1.547	0.255	-1.851
10x2	-1.501	0.348	0.967	0.109
10x10	0.000	0.000	0.000	0.000
15x1	-4.636	-1.369	0.357	-1.698
15x2	-1.204	0.641	1.136	0.343
20x1	-4.677	-1.290	0.316	-1.710
20x2	-1.185	0.679	0.977	0.291
30x1	-4.525	-1.179	0.470	-1.571
30x2	-0.917	0.719	0.988	0.388
40x1	-4.529	-1.312	0.320	-1.676
40x2	-0.797	0.759	1.053	0.463

Table **4-1** shows the percentage difference between the average measured OPF compared to the literature value. All fields are defined using jaws only. See Appendix A.1 for the complete data set.

Table 4-2: Cumulative Percentage Differences (%) when Comparing Measured and Eclipse OPFs by Field Size, MLC Shaped Fields

Average Measured OPF to Literature Percent Differences (%) - MLCs				
Field Size (cm)	Exradin A16	Sun Nuclear Edge	IBA Razor	Cumulative
1x1	0.898	0.537	1.008	-0.808
1x2	0.217	0.958	1.956	-1.033
1x3	0.031	1.255	2.600	-1.279
2x1	-0.597	0.907	1.878	-0.724
2x2	-2.210	-0.799	0.727	0.767
2x3	-1.974	-0.618	0.729	0.625
3x1	-0.714	1.220	2.803	-1.091
3x2	-2.115	-0.670	0.390	0.805
3x3	-2.131	-0.722	0.481	0.797
10x10	0.000	0.000	0.000	0.000

Table **4-2** shows the percentage difference between the average measured OPFs compared to the Eclipse values. All fields are defined using MLCs, with jaws tracking 0.5cm behind MLCs. See Appendix A.2 for the complete data set.

CHAPTER 5. DISCUSSION

5.1 Interpretation of Results

5.1.1 Jaw Measurements

In this section, the results of the jaw-defined field measurements using the Exradin A16, Sun Nuclear EDGE diode, and IBA Razor diode are examined. These detectors were used to assess the new AXBe OPFs for different jaw-shaped fields. Each detector's data is presented and compared against the expected OPFs to determine how well the new values align with the existing reference data. The discussion focuses on the consistency across different detectors and any notable variations in the results for each field size.

5.1.1.1 Exradin A16 Ion Chamber

The Exradin A16 Ion chamber was the ideal ion chamber for this experiment due to the availability of the detector, the accessibility of published output correction factors in TRS-483, and its small active volume of 0.07cc. Upon analysing the jaw OPF measurements, the Exradin A16 data appears to be the most inconsistent of the three detectors. While many of the measurements are within the +/- 2% range, and only two measurements fall between 2% and 3%, there are a total of 10 field sizes with measured OPFs outside of the 3% limit this study hoped for. Upon further evaluation, all red measurements (>3% difference) are less than 5% and are all negative. This suggests that the Exradin A16 is recording lower than expected OPFs. It is also important to note that all the red readings were recorded on fields that had a Y-Jaw size of 1cm (2x1, 3x1, 4x1, etc.). Though it would be ideal for all the measurements to have been within less than 3%, this was expected

according to the published data. In fact, Sun Nuclear uses this exact discrepancy in the A16 for small fields to promote the Edge detector.[14]

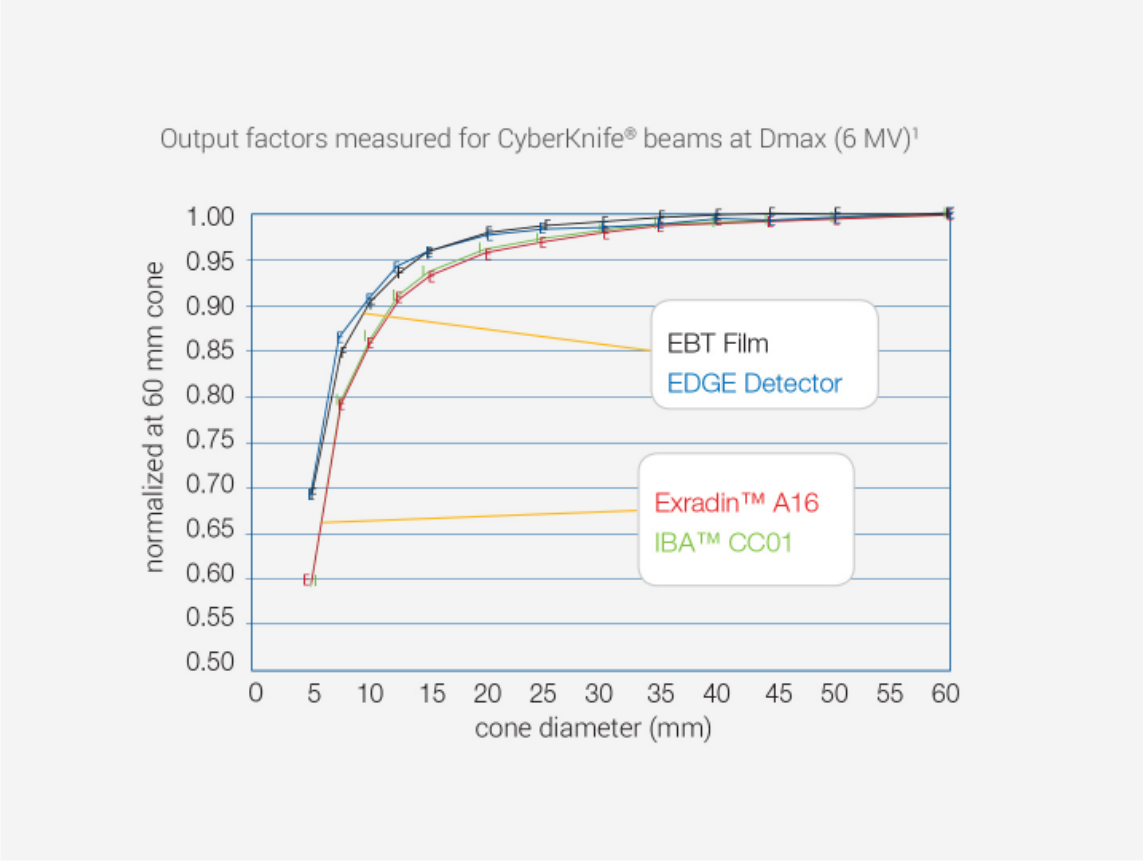

Figure 5-1: Measured OPFs for several detectors on the Cyberknife 6MV, cone-based delivery, according to Sun Nuclear

While the above figure is collected using a CyberKnife cone and 6MV beams, the concept of the A16 reporting lower-than-expected OPFs at smaller field sizes, especially for fields 1cm and smaller, is still apparent. This is further reinforced by the data collected in this study. Nearly every OPF measured by the A16 was cold compared to the expected values, with the differences most significant for the 1cm fields. The only exceptions to this were the 2x20, 2x30, and 2x40, which had very slightly positive differences (all less than +0.3%). The measurements for the A16 were expected to be cold, and most measurements

were within acceptable tolerance, however, this data was not strong enough to validate the AXBe model of its own due to the large differences noted.

5.1.1.2 Sun Nuclear Edge Diode

The Edge Diode was expected to be the ideal detector available for this study. Again, output correction factors were readily available in TRS-483. The manual states an active detection volume of 0.019cc, with very accurate OPF measurements down to 0.05cm fields.[14] Furthermore, it is one of the recommended diodes from the BP^2 water tank manual.[18] The OPF measurements with this detector strongly agree with the AXBe model. Only 3 measurements were in the yellow range, and none were red. Of those in the yellow, the greatest was only over by 0.1%. As opposed to the A16, where most measurements appeared cold, there seems to be no such pattern for the Edge detector, as the readings range from +2.057% to -2.104%. This strongly supports the accuracy of the AXBe model, as all measurements were within limit for this detector.

5.1.1.3 IBA Razor Diode

The IBA Razor was selected as the final detector for this study to provide variety. It was the only detector used that was not presented in TRS-483, and the only detector that required positioning to be in parallel to the beam. The Razor diode was also made by the same company as the BP^2 water tank (IBA), and therefore was also a recommended diode from the manual. While the IBA Razor Nano ion chamber was considered, the literature published correction factors were too scarce to provide a reliable spline interpolation for small fields.[16] Furthermore, due to the nature of small fields and recommendations from TRS-483, a second diode was preferable as opposed to a second ion chamber. The data

collected from this detector was similar to the Sun Nuclear Edge Diode, with no measurements recorded in the red. There was, however, a series of 7 measurements that were in the yellow range. It is noted that, overall, the measurements of this detector tended to overestimate the OPFs, and all yellow readings appeared to be hotter than expected. The data collected from the Razor diode was completely within limits, again supporting the AXBe model.

5.1.1.4 Cumulative Jaw Data

After collecting OPFs for each field on all three detectors, the OPFs were then averaged and compared to both the AXBe model and the OPFs obtained by Eclipse. A percent difference was also obtained between the Eclipse and AXBe OPFs just to confirm cohesion between the beam model, the TPS, and the delivery of the beam. Of note, all Eclipse OPFs were within 2% of the AXBe beam model. Furthermore, all averaged OPFs were within tolerance of both the Eclipse and AXBe OPFs, with only 4 fields having yellow measurements. These fields were the 3x1, 4x1, 5x1, and 10x1, and were all cold compared to the expected value. As these were some of the worst recorded OPFs for the A16, this was to be expected. The data shown here strongly supports the accuracy of the AXBe model, as the only measurements outside of the limits were expected from the published data, while the Sun Nuclear Edge, IBA Razor, and averaged data were all within tolerance. Furthermore, when including a standard deviation error to the averaged data, the comparison to both the Eclipse and AXBe OPFs shows minimal deviation, as seen below.

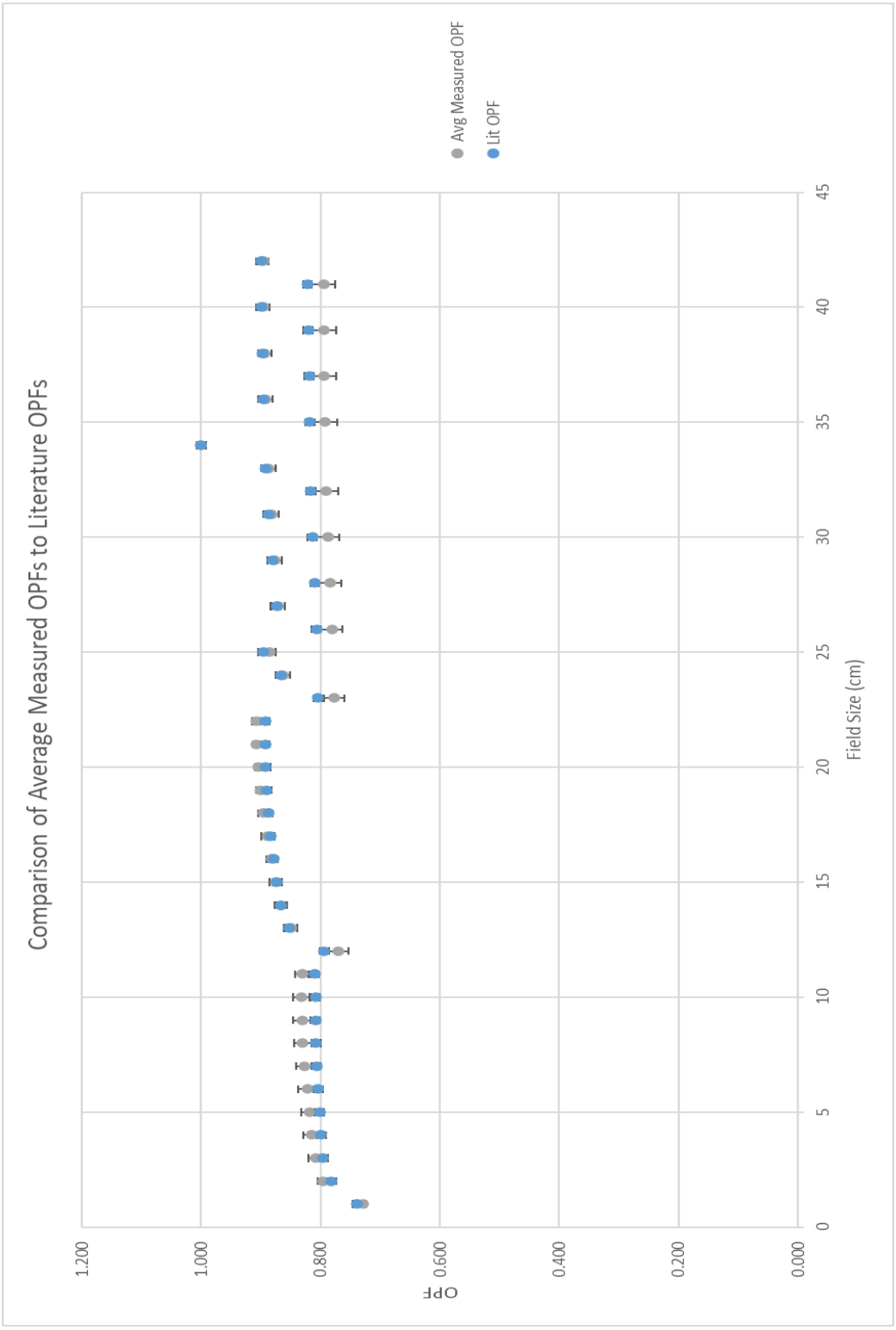

Figure 5-2: Comparison of the average measured OPF with error bars of 1 standard deviation, by field size, compared to the AXBe literature values

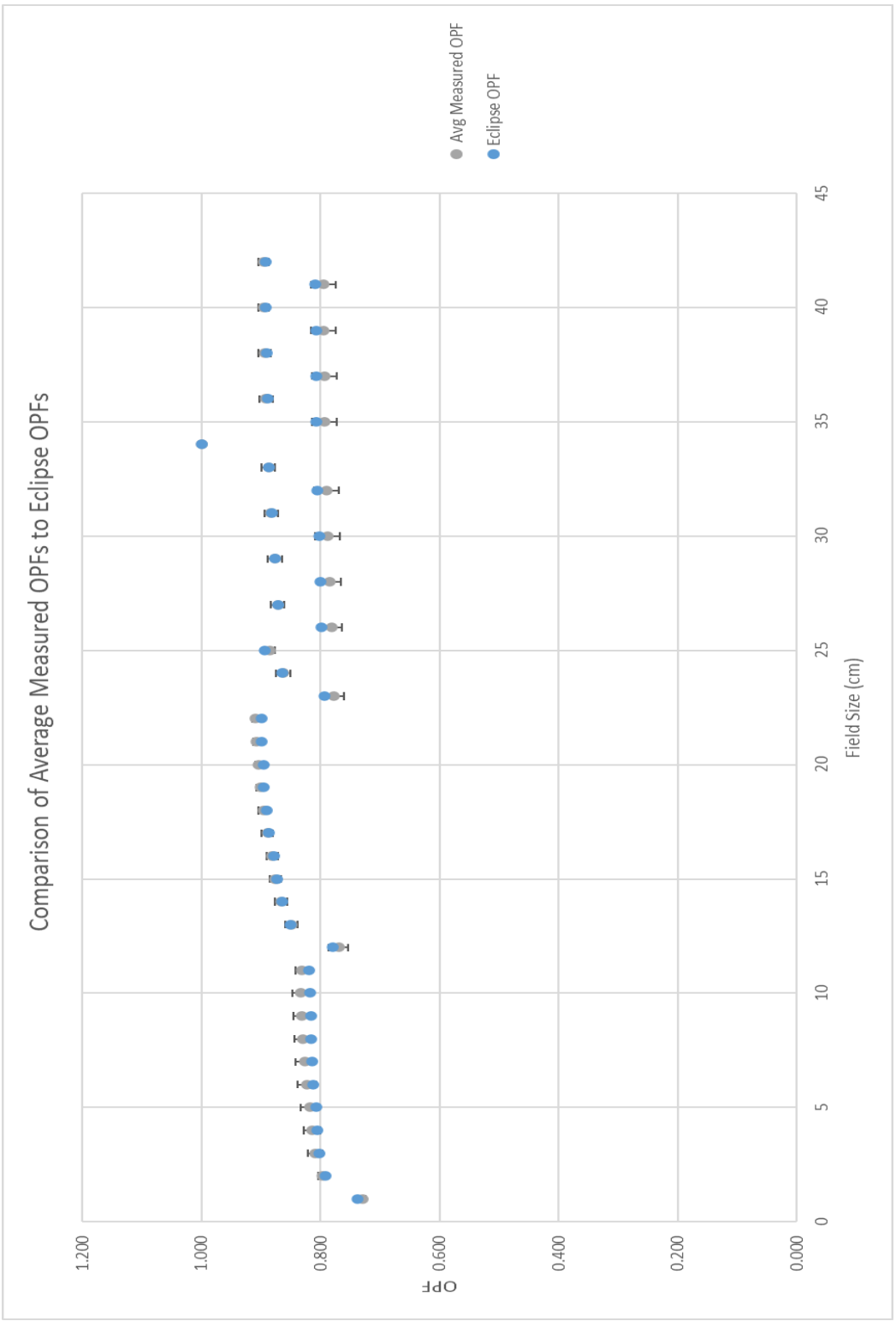

Figure 5-3: Comparison of the average measured OPF with error bars of 1 standard deviation, by field size, compared to the Eclipse measured values

5.1.1.5 MLC Measurements

In the measurements taken for creating the AXBe model, Ning Wu states all field measurements were recorded using jaw-defined fields only. They go on to suggest future studies utilizing MLC planning. Since all SRT plans on the Edge are VMAT, MLC measurements were taken to better confirm the validity of the AXBe model. Since the Edge uses dynamic jaw tracking, MLC fields were created at the desired field size with jaws 0.5cm retracted, creating a 1cm difference between the MLC field and the jaw size (a 1x1cm MLC field has a 2x2 jaw size). Since literature OPFs were not provided, the measured OPFs were only compared to the Eclipse OPFs for these fields. Measurements were not taken for any field length greater than 3cm, except for the 10x10 field for reference. This was done due to the nature of the AXBe model only changing OPFs for fields smaller than 3cm, and that SRT plans generally do not use large irregular MLCs (such as a 1x40cm). All measurements for all detectors showed OPFs well within limits, with the greatest average difference being -1.279%. This again confirms the validity of the AXBe model, showing strong congruence with both the jaw-defined fields and MLC planned fields as well.

5.2 Clinical Impact and Relevance

To address the clinical impact of introducing the AXBe model, 9 SRS plans from a retrospective study were analyzed using both the AXB and AXBe models. The goal of this comparison was two-fold. First, all validation performed so far was completed using static, single fields. Applying the AXBe model to a VMAT SRT plan aids in validating that the

model works smoothly in a dynamic plan. Secondly, the hope is to show that the AXBe model better represents the planned and delivered doses of small fields through extending the OPF table.

The goal of this retrospective analysis is to address only the impact of changing the beam model. For all 9 plans, the original plan and QA were copied into a new course and the patient ID was randomized to act as the control. This plan was then copied again, the beam model was changed from AXB 15.6 to the AXBe model, the plan was recalculated (but not re-optimized), and a QA plan was created for the new plan. The first comparison between the AXB and AXBe model was made using a script in Eclipse called ClearCheck, created by RADformation. This script is used on all SRT plans at this clinic and helps to analyze dose distribution, conformality, and OAR avoidance, as seen in Figure 5-4. This figure shows that, for both the original and new plan, all the parameters remain acceptable. However, it also shows that the total absolute hot and cold spots of the AXBe model were closer to the planned dose, leading to an improved conformality index. This improvement in conformality is shown throughout all 9 Clear Checks, as can be seen in Appendix 2.

Priority	Structure Template	Structure Plan	Type	Prescription	Constraint	Goal	MultiMets	AXBe 98706	Difference	Pass/Fail
1	PTV_1	PTV_Left occipital	Target	**Total Dose: 2100cGy**	V100% ≥	95%	99.958%	99.932%	0.026	✓
2	PTV_1	PTV_Left occipital	Target	**Total Dose: 2100cGy**	V95% ≥	100%	100%	100%	0	✓
3	PTV_1	PTV_Left occipital	Target	**Total Dose: 2100cGy**	D0.035cc ≤ (HI)	130%	126.403%	126.332%	0.071	✓
4	PTV_1	PTV_Left occipital	Target	**Total Dose: 2100cGy**	**CI using PTV_Left occipital 1(**	1.2-1.5	1.15	1.135	0.015	✓
5	PTV_2	PTV_Left temporal	Target	**Total Dose: 2100cGy**	V100% ≥	95%	99.578%	99.821%	-0.243	✓
6	PTV_2	PTV_Left temporal	Target	**Total Dose: 2100cGy**	V95% ≥	100%	100%	100%	0	✓
7	PTV_2	PTV_Left temporal	Target	**Total Dose: 2100cGy**	D0.035cc ≤ (HI)	130%	125.837%	125.902%	-0.065	✓
8	PTV_2	PTV_Left temporal	Target	**Total Dose: 2100cGy**	**CI using PTV_Left temporal 1**	1.2-1.5	1.208	1.195	0.013	AXBe 98706
9	PTV_3	PTV_Right frontal	Target	**Total Dose: 2100cGy**	V100% ≥	95%	99.995%	99.999%	-0.004	✓
10	PTV_3	PTV_Right frontal	Target	**Total Dose: 2100cGy**	V95% ≥	100%	100%	100%	0	✓
11	PTV_3	PTV_Right frontal	Target	**Total Dose: 2100cGy**	D0.035cc ≤ (HI)	130%	125.577%	125.442%	0.135	✓
12	PTV_3	PTV_Right frontal	Target	**Total Dose: 2100cGy**	**CI using PTV_Right frontal 1(**	1.2-1.5	1.223	1.206	0.017	△
13	Brainstem	BrainStem	OAR		D0.035cc ≤	1500cGy	336.8cGy	332.9cGy	3.9	✓
14	Brainstem	BrainStem	OAR		D0.5cc ≤	1000cGy	277.5cGy	274.7cGy	2.8	✓
15	Chiasm	Chiasm	OAR		D0.035cc ≤	1000cGy	167.8cGy	164.4cGy	3.4	✓
16	Cochlea_L	Cochlea_L	OAR		Max ≤	900cGy	146.3cGy	148.2cGy	-1.9	✓
17	Cochlea_L	Cochlea_L	OAR		Mean ≤ (Optimal)	400cGy	117.6cGy	117.9cGy	-0.3	✓
18	Cochlea_L	Cochlea_L	OAR		Mean ≤ (Mandatory)	900cGy	117.6cGy	117.9cGy	-0.3	✓
19	Cochlea_R	Cochlea_R	OAR		Max ≤	900cGy	186.1cGy	186.1cGy	0	✓
20	Cochlea_R	Cochlea_R	OAR		Mean ≤ (Optimal)	400cGy	156.8cGy	157.9cGy	-1.1	✓
21	Cochlea_R	Cochlea_R	OAR		Mean ≤ (Mandatory)	900cGy	156.8cGy	157.9cGy	-1.1	✓
22	Eye_L	Eye_L	OAR		D0.035cc ≤	500cGy	126.3cGy	125.1cGy	1.2	✓
23	Eye_R	Eye_R	OAR		D0.035cc ≤	500cGy	101.6cGy	101.5cGy	0.1	✓

Figure 5-4: Clear Check for case 98706

Finally, each original plan was then run on the Edge in QA mode and recorded using the Sun Nuclear SRS-MapCHECK phantom and software. Once the original plan was run, it was then compared to both the original QA and the new AXBe QA.

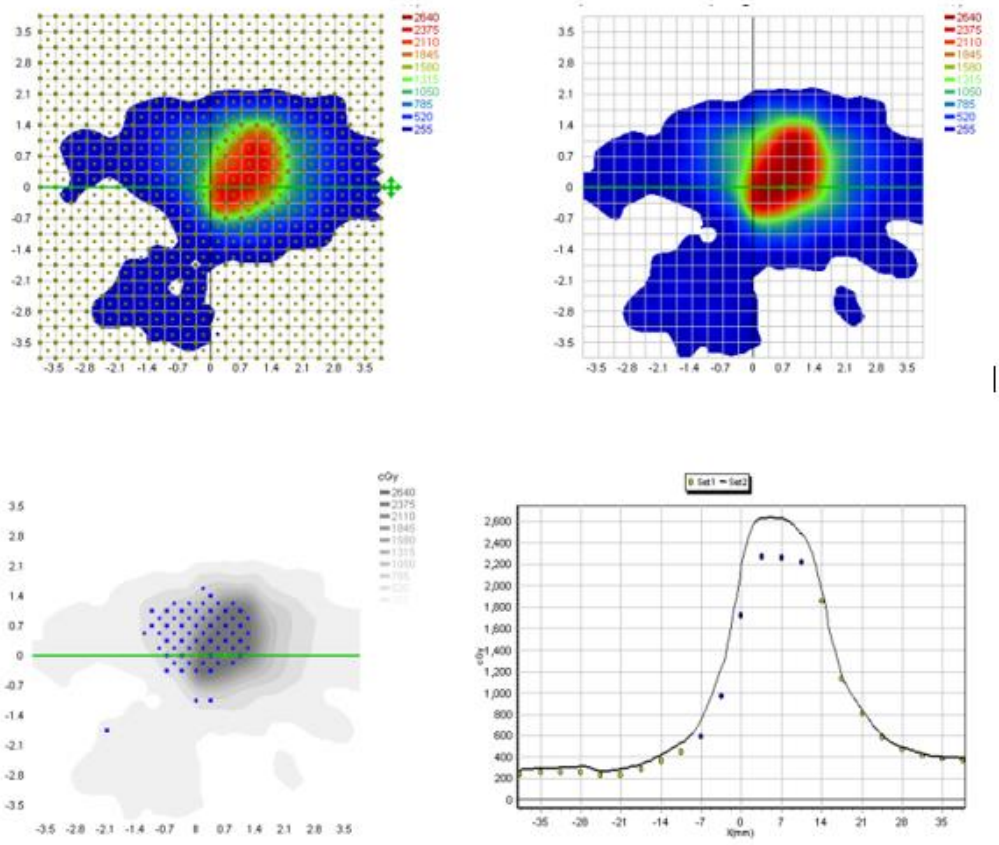

Summary (Gamma Analysis)

Pass (%)	85.3
Pass	388
Fail	67
Total Points	455

Figure 5-5: SRS-MapCheck QA for case 98706 original plan

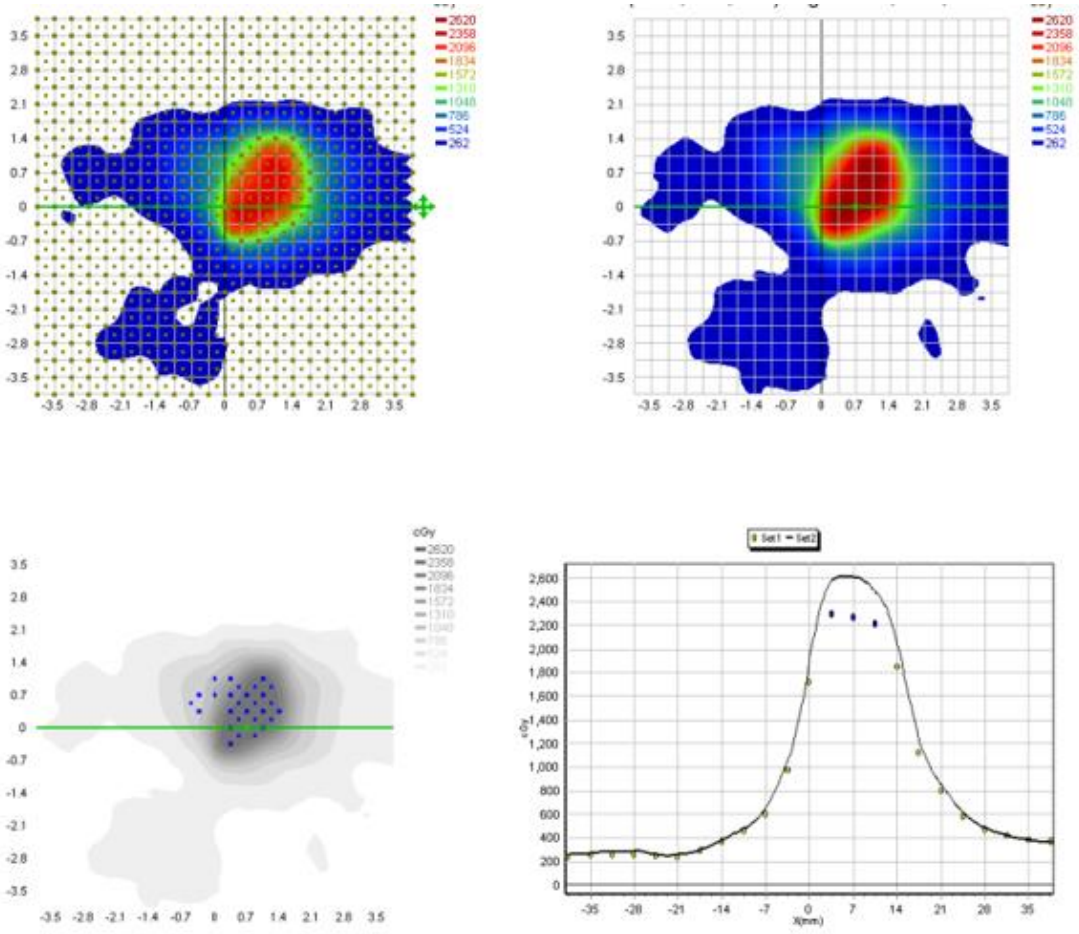

Pass (%)	93.5
Pass	418
Fail	29
Total Points	447

Figure 5-6: SRS MapCheck QA for case 98706 new AXBe plan

As can be seen from figures 5-5 and 5-6, simply changing the beam model from AXB15.6 to AXBe showed a significant improvement in the QA results. Since both plans were created using the exact same optimization and compared using the same delivered plan, this helps to show the improvement in dose calculation performance on small fields with

the new AXBe model. Clinically, while there was no change in the plan delivered between the two QAs, this suggests that AXBe may improve confidence between the plan created in Eclipse and the dose distribution that a patient receives. The first 5 cases analyzed all showed cold spots on the original QAs, and the last 4 were originally accurate to the planned distribution. Upon reviewing all the new QAs, all 5 cold plans showed at least minor improvements to the pass rate and reductions in the degree of the cold spots measured. When comparing the final 4 plans, it is of note that, while all 4 plans did pass using AXBe, two of the plans were slightly hot in comparison. This retrospective analysis suggests that the AXBe model is likely to provide a more accurate calculation and representation of the dose distribution for SRT plans.

5.3 Limitations of the Study

This study was limited to data collected from the Varian Edge at Morton Plant hospital, using the 6xFFF beam energy. While this data may be of use to other clinical centers, the intent of this study is only to verify the use of AXBe on this machine. The clinical goal will be to apply the AXBe OPFs for SRT planning only. Furthermore, this study is limited to only confirming the validity of the AXBe model and is not designed to refine or make alterations to the published data. This study was limited to using only the detectors and materials available to the clinic. Furthermore, this study was limited to using only retrospective SRS data collected for treatments delivered via the Edge.

5.4 Suggestions for Future Research

While the data collected does support the literature data, this study could be improved in the future by recreating the initial research parameters more closely. For example, the

initial AXBe model was created using a scintillator detector, which would have been ideal to use for this study had one been available. However, the agreement seen between data collected across several detectors helps to confirm the reproducibility of the original data.

This data could also be expanded upon if desired, applying a similar approach to the other energies available on the Varian Edge. This clinic hopes to begin a trigeminal neuralgia program in the near future, which will likely be a cone-based system. Due to the extremely small field sizes, it may be worthwhile repeating a similar process using the cones.

For comparing OPFs, there are some steps that could be taken to confirm that the AXBe model is more accurate than the original base AXB model. First, OPFs measured during this study were made to confirm agreement between the measured OPFs and literature data for the AXBe model. However, measurements were not taken using the current AXB model. By repeating the Eclipse planning used in this study, Eclipse-calculated AXB OPFs for fields smaller than 3x3 could be measured for comparison as well. This could help quantify the improvement made by the AXBe model, giving clinics in the future insight as to how worthwhile incorporating AXBe might be. Additionally, an end-to-end test could be performed with and without the AXBe model if desired.

It is important to note that the AXBe model only makes changes to fields that are smaller than 3cm. Many of the SRT plans likely have many control points with field sizes both larger and smaller than the 3cm field size. This means that incorporating the AXBe model could potentially make little to no difference depending on the tumor and field size. Analysis of the PTV volume size and control point data may help to quantify the impact of the AXBe model by determining what percentage of the plan was utilizing the new OPFs.

Finally, a clinical study could be used to compare the AXBe and AXB models for SRT plans. The current retrospective analysis was done by only recalculating the original plan, without the use of re-optimization. This was done intentionally for this study as it would be difficult to reproduce the specific optimization patterns that may have been used by the dosimetrists during planning. Therefore, it is hard to conclude if treatment plans made using the AXBe model alone would make an overall improvement over those made using AXB. A possible solution to this would be to have the same planning team continue planning SRT treatments using AXB, but to additionally create a second plan using the AXBe model at the same time. By doing so, a long-term clinical comparison could be made by comparing the average plan quality over a given time. While this would essentially create twice as much work for each plan, it would provide a more accurate comparison of the two models.

CHAPTER 6. CONCLUSION

6.1 Summary of Findings

This study supports the validity of using the AXBe model for calculating small-field output factors (OPFs). Despite some questionable readings from the A16 Micro ion chamber, the findings demonstrate that a combination of ion chamber and diode detectors is effective for small field measurements, offering a viable alternative to scintillator detectors.

Moreover, the retrospective data indicates that the extended OPF table yields more accurate and conformal dose predictions, highlighting the AXBe model's potential effectiveness for stereotactic radiotherapy (SRT) planning. Conducting a long-term clinical study to compare treatment plans generated using the AXB and AXBe models could provide valuable insights into the advantages of the extended OPF table for SRT applications.

APPENDIX A. OPF MEASUREMENTS

A.1 Jaw-Only OPFs

Table A-1: OPF Measurements using Exradin A16 Micro Ion Chamber (Jaws)

Exradin A16 Measurements Jaws

Field Size (cm)	Reading 1 (nC)	Reading 2 (nC)	Reading 3 (nC)	Avg (nC)	Correction Factor	Corrected Avg (nC)	10x10 Avg (nC)	Measured OPF	Lit OPF	lit % diff
1x1	0.153	0.153	0.153	0.153	1.027	0.157	0.217	0.724	0.739	-2.030
1x2	0.169	0.169	0.169	0.169	1.012	0.171	0.217	0.787	0.794	-0.889
1x3	0.171	0.171	0.172	0.171	1.008	0.173	0.217	0.795	0.804	-1.103
1x4	0.172	0.172	0.173	0.172	1.006	0.173	0.217	0.799	0.807	-1.015
1x5	0.173	0.173	0.174	0.173	1.005	0.174	0.217	0.801	0.810	-1.099
1x7	0.174	0.174	0.175	0.174	1.005	0.175	0.217	0.806	0.814	-0.959
1x10	0.175	0.175	0.176	0.175	1.004	0.176	0.217	0.809	0.816	-0.828
1x15	0.176	0.176	0.177	0.176	1.004	0.177	0.217	0.814	0.818	-0.524
1x20	0.176	0.176	0.177	0.176	1.003	0.177	0.217	0.815	0.819	-0.500
1x30	0.177	0.177	0.177	0.177	1.003	0.177	0.217	0.817	0.821	-0.498
1x40	0.177	0.177	0.178	0.177	1.003	0.178	0.217	0.818	0.822	-0.450
2x1	0.162	0.162	0.162	0.162	1.012	0.164	0.217	0.754	0.782	-3.523
2x2	0.181	0.182	0.181	0.181	1.003	0.182	0.217	0.838	0.853	-1.793
2x3	0.186	0.185	0.185	0.185	1.001	0.186	0.217	0.855	0.867	-1.408
2x4	0.188	0.187	0.187	0.187	1.001	0.188	0.217	0.864	0.874	-1.107
2x5	0.189	0.189	0.189	0.189	1.000	0.189	0.217	0.871	0.881	-1.171
2x7	0.190	0.191	0.191	0.191	1.000	0.191	0.217	0.879	0.888	-1.051
2x10	0.192	0.192	0.193	0.192	1.000	0.192	0.217	0.886	0.892	-0.617
2x15	0.194	0.194	0.194	0.194	1.000	0.194	0.217	0.893	0.896	-0.306
2x20	0.195	0.195	0.195	0.195	1.000	0.195	0.217	0.897	0.897	0.011
2x30	0.195	0.196	0.195	0.196	1.000	0.196	0.217	0.901	0.900	0.121
2x40	0.196	0.196	0.196	0.196	1.000	0.196	0.217	0.903	0.900	0.292
3x1	0.164	0.163	0.163	0.163	1.008	0.165	0.217	0.759	0.796	-4.641
3x2	0.185	0.184	0.184	0.184	1.001	0.185	0.217	0.850	0.866	-1.809
3x3	0.190	0.189	0.190	0.190	1.000	0.190	0.217	0.875	0.896	-2.346
4x1	0.164	0.164	0.165	0.164	1.006	0.165	0.217	0.762	0.799	-4.627
4x2	0.186	0.186	0.187	0.186	1.001	0.186	0.217	0.859	0.873	-1.628
5x1	0.165	0.165	0.165	0.165	1.005	0.166	0.217	0.764	0.802	-4.770
5x2	0.187	0.187	0.188	0.187	1.000	0.187	0.217	0.863	0.879	-1.768
7x1	0.165	0.165	0.166	0.166	1.005	0.166	0.217	0.767	0.804	-4.642
7x2	0.188	0.188	0.189	0.189	1.000	0.189	0.217	0.869	0.884	-1.680
10x1	0.166	0.166	0.167	0.166	1.004	0.167	0.217	0.768	0.807	-4.843
10x2	0.190	0.190	0.190	0.190	1.000	0.190	0.217	0.875	0.888	-1.501
10x10	0.217	0.216	0.217	0.217	1.000	0.217	0.217	1.000	1.000	0.000
15x1	0.166	0.167	0.166	0.167	1.004	0.167	0.217	0.771	0.808	-4.636
15x2	0.191	0.191	0.191	0.191	1.000	0.191	0.217	0.879	0.890	-1.204
20x1	0.167	0.167	0.167	0.167	1.003	0.167	0.217	0.771	0.809	-4.677
20x2	0.191	0.192	0.191	0.191	1.000	0.191	0.217	0.881	0.892	-1.185
30x1	0.167	0.168	0.167	0.167	1.003	0.168	0.217	0.772	0.809	-4.525
30x2	0.192	0.192	0.192	0.192	1.000	0.192	0.217	0.885	0.893	-0.917
40x1	0.168	0.167	0.167	0.167	1.003	0.168	0.217	0.773	0.810	-4.529
40x2	0.193	0.192	0.192	0.192	1.000	0.192	0.217	0.886	0.893	-0.797

Table A-2: OPF Measurements using Sun Nuclear EDGE Diode Detector (Jaws)

Sun Nuclear EDGE Measurements Jaws

Field Size (cm)	Reading 1 (nC)	Reading 2 (nC)	Reading 3 (nC)	Avg (nC)	Correction Factor	Corrected Avg (nC)	10x10 Avg (nC)	Measured OPF	Lit OPF	lit % diff
1x1	27.760	27.770	27.770	27.767	0.966	26.823	36.753	0.730	0.739	-1.245
1x2	29.910	29.930	29.910	29.917	0.981	29.348	36.753	0.799	0.794	0.569
1x3	30.260	30.250	30.290	30.267	0.986	29.843	36.753	0.812	0.804	0.992
1x4	30.420	30.450	30.430	30.433	0.988	30.068	36.753	0.818	0.807	1.376
1x5	30.530	30.550	30.530	30.537	0.990	30.231	36.753	0.823	0.810	1.549
1x7	30.680	30.690	30.680	30.683	0.991	30.407	36.753	0.827	0.814	1.638
1x10	30.800	30.790	30.800	30.797	0.992	30.550	36.753	0.831	0.816	1.866
1x15	30.860	30.880	30.900	30.880	0.993	30.664	36.753	0.834	0.818	1.994
1x20	30.930	30.950	30.930	30.937	0.993	30.720	36.753	0.836	0.819	2.057
1x30	30.990	30.990	30.990	30.990	0.993	30.773	36.753	0.837	0.821	1.984
1x40	31.040	31.040	31.020	31.033	0.993	30.816	36.753	0.838	0.822	2.002
2x1	28.780	28.780	28.770	28.777	0.981	28.230	36.753	0.768	0.782	-1.779
2x2	31.470	31.460	31.450	31.460	0.994	31.271	36.753	0.851	0.853	-0.253
2x3	31.990	32.040	32.050	32.027	0.997	31.931	36.753	0.869	0.867	0.205
2x4	32.330	32.330	32.320	32.327	0.999	32.294	36.753	0.879	0.874	0.535
2x5	32.520	32.530	32.540	32.530	0.999	32.497	36.753	0.884	0.881	0.364
2x7	32.780	32.790	32.820	32.797	0.999	32.764	36.753	0.891	0.888	0.389
2x10	33.050	33.070	33.030	33.050	0.999	33.017	36.753	0.898	0.892	0.711
2x15	33.210	33.200	33.170	33.193	1.000	33.193	36.753	0.903	0.896	0.797
2x20	33.290	33.290	33.320	33.300	1.000	33.300	36.753	0.906	0.897	1.008
2x30	33.360	33.400	33.370	33.377	1.000	33.377	36.753	0.908	0.900	0.903
2x40	33.420	33.460	33.410	33.430	1.000	33.430	36.753	0.910	0.900	1.064
3x1	29.060	29.040	29.040	29.047	0.986	28.640	36.753	0.779	0.796	-2.104
3x2	31.920	31.900	31.900	31.907	0.997	31.811	36.753	0.866	0.866	-0.055
3x3	32.650	32.670	32.650	32.657	0.999	32.624	36.753	0.888	0.896	-0.932
4x1	29.150	29.180	29.160	29.163	0.988	28.813	36.753	0.784	0.799	-1.882
4x2	32.220	32.210	32.190	32.207	0.999	32.174	36.753	0.875	0.873	0.277
5x1	29.240	29.250	29.260	29.250	0.990	28.958	36.753	0.788	0.802	-1.760
5x2	32.380	32.390	32.410	32.393	0.999	32.361	36.753	0.880	0.879	0.170
7x1	29.340	29.360	29.390	29.363	0.991	29.099	36.753	0.792	0.804	-1.525
7x2	32.630	32.600	32.670	32.633	0.999	32.601	36.753	0.887	0.884	0.341
10x1	29.410	29.460	29.440	29.437	0.992	29.201	36.753	0.795	0.807	-1.547
10x2	32.750	32.800	32.800	32.783	0.999	32.751	36.753	0.891	0.888	0.348
10x10	36.750	36.750	36.760	36.753	1.000	36.753	36.753	1.000	1.000	0.000
15x1	29.490	29.490	29.510	29.497	0.993	29.290	36.753	0.797	0.808	-1.369
15x2	32.910	32.920	32.930	32.920	1.000	32.920	36.753	0.896	0.890	0.641
20x1	29.560	29.550	29.560	29.557	0.993	29.350	36.753	0.799	0.809	-1.290
20x2	33.010	33.020	32.990	33.007	1.000	33.007	36.753	0.898	0.892	0.679
30x1	29.570	29.620	29.580	29.590	0.993	29.383	36.753	0.799	0.809	-1.179
30x2	33.080	33.020	33.070	33.057	1.000	33.057	36.753	0.899	0.893	0.719
40x1	29.580	29.580	29.600	29.587	0.993	29.380	36.753	0.799	0.810	-1.312
40x2	33.070	33.060	33.080	33.070	1.000	33.070	36.753	0.900	0.893	0.759

Table A-3: OPF Measurements using IBA Razor Diode Detector (Jaws)

IBA Razor Diode Measurements Jaws

Field Size (cm)	Reading 1 (nC)	Reading 2 (nC)	Reading 3 (nC)	Avg (nC)	Correction Factor	Corrected Avg (nC)	10x10 Avg (nC)	Measured OPF	Lit OPF	lit % diff
1x1	3.014	3.017	3.009	3.013	1.007	3.034	4.134	0.734	0.739	-0.666
1x2	3.246	3.248	3.248	3.247	1.022	3.319	4.134	0.803	0.794	1.116
1x3	3.287	3.290	3.295	3.291	1.029	3.386	4.134	0.819	0.804	1.884
1x4	3.311	3.310	3.317	3.313	1.031	3.415	4.134	0.826	0.807	2.383
1x5	3.327	3.322	3.321	3.323	1.032	3.430	4.134	0.830	0.810	2.431
1x7	3.343	3.340	3.337	3.340	1.033	3.450	4.134	0.835	0.814	2.538
1x10	3.359	3.357	3.357	3.358	1.032	3.465	4.134	0.838	0.816	2.729
1x15	3.369	3.372	3.370	3.370	1.032	3.478	4.134	0.841	0.818	2.864
1x20	3.376	3.375	3.376	3.376	1.032	3.484	4.134	0.843	0.819	2.901
1x30	3.381	3.382	3.383	3.382	1.031	3.487	4.134	0.844	0.821	2.743
1x40	3.388	3.381	3.390	3.386	1.022	3.461	4.134	0.837	0.822	1.853
2x1	3.153	3.150	3.156	3.153	1.031	3.251	4.134	0.786	0.782	0.564
2x2	3.447	3.440	3.456	3.448	1.029	3.548	4.134	0.858	0.853	0.613
2x3	3.518	3.523	3.518	3.520	1.028	3.618	4.134	0.875	0.867	0.958
2x4	3.556	3.557	3.562	3.558	1.027	3.654	4.134	0.884	0.874	1.151
2x5	3.588	3.587	3.580	3.585	1.025	3.675	4.134	0.889	0.881	0.902
2x7	3.628	3.625	3.620	3.624	1.024	3.711	4.134	0.898	0.888	1.107
2x10	3.646	3.652	3.652	3.650	1.022	3.730	4.134	0.902	0.892	1.168
2x15	3.672	3.671	3.670	3.671	1.021	3.748	4.134	0.907	0.896	1.197
2x20	3.685	3.689	3.684	3.686	1.019	3.756	4.134	0.909	0.897	1.298
2x30	3.700	3.705	3.703	3.703	1.019	3.773	4.134	0.913	0.900	1.417
2x40	3.704	3.710	3.709	3.708	1.019	3.778	4.134	0.914	0.900	1.554
3x1	3.192	3.191	3.185	3.189	1.029	3.282	4.134	0.794	0.796	-0.261
3x2	3.510	3.506	3.512	3.509	1.029	3.611	4.134	0.874	0.866	0.876
3x3	3.604	3.605	3.608	3.606	1.026	3.699	4.134	0.895	0.896	-0.117
4x1	3.202	3.201	3.202	3.202	1.031	3.301	4.134	0.799	0.799	-0.057
4x2	3.547	3.548	3.545	3.547	1.028	3.646	4.134	0.882	0.873	1.033
5x1	3.209	3.214	3.214	3.212	1.032	3.315	4.134	0.802	0.802	-0.002
5x2	3.571	3.574	3.567	3.571	1.027	3.667	4.134	0.887	0.879	0.924
7x1	3.226	3.229	3.225	3.227	1.033	3.333	4.134	0.806	0.804	0.291
7x2	3.600	3.592	3.595	3.596	1.025	3.686	4.134	0.892	0.884	0.859
10x1	3.242	3.242	3.238	3.241	1.032	3.344	4.134	0.809	0.807	0.255
10x2	3.614	3.622	3.622	3.619	1.024	3.706	4.134	0.897	0.888	0.967
10x10	4.130	4.134	4.137	4.134	1.000	4.134	4.134	1.000	1.000	0.000
15x1	3.245	3.252	3.247	3.248	1.032	3.352	4.134	0.811	0.808	0.357
15x2	3.639	3.640	3.643	3.641	1.022	3.721	4.134	0.900	0.890	1.136
20x1	3.250	3.254	3.248	3.251	1.032	3.355	4.134	0.812	0.809	0.316
20x2	3.645	3.649	3.646	3.647	1.021	3.723	4.134	0.901	0.892	0.977
30x1	3.254	3.256	3.257	3.256	1.032	3.360	4.134	0.813	0.809	0.470
30x2	3.661	3.657	3.657	3.658	1.019	3.728	4.134	0.902	0.893	0.988
40x1	3.257	3.260	3.257	3.258	1.031	3.359	4.134	0.813	0.810	0.320
40x2	3.659	3.660	3.663	3.661	1.019	3.730	4.134	0.902	0.893	1.053

Table A-4: Cumulative OPF Measurementts (Jaws)

Cumulative OPF Jaws

Field Size (cm)	Eq. Square (cm)	Lit OPF	Exclipse 10x10 Dose (cGy)	Eclipse Field Dose (cGy)	Eclipse OPF	Eclipse to Lit %Diff	Avg Measured OP	Avg OPF Error (SD)	Avg literature %diff	Avg Eclipse %diff
1x1	1.000	0.739	92.500	68.200	0.737	-0.230	0.729	0.005	-1.314	-1.086
1x2	1.330	0.782	92.500	73.200	0.791	1.196	0.796	0.008	0.265	0.601
1x3	1.500	0.796	92.500	74.200	0.802	0.774	0.809	0.012	0.591	0.822
1x4	1.600	0.799	92.500	74.500	0.805	0.802	0.814	0.014	0.915	1.114
1x5	1.670	0.802	92.500	74.700	0.808	0.694	0.818	0.015	0.960	1.265
1x7	1.750	0.804	92.500	75.100	0.812	0.982	0.823	0.015	1.072	1.335
1x10	1.820	0.807	92.500	75.300	0.814	0.874	0.826	0.015	1.256	1.498
1x15	1.880	0.808	92.500	75.500	0.816	1.017	0.830	0.014	1.445	1.667
1x20	1.900	0.809	92.500	75.500	0.816	0.892	0.831	0.015	1.486	1.832
1x30	1.940	0.809	92.500	75.700	0.818	1.159	0.833	0.014	1.410	1.735
1x40	1.950	0.810	92.500	75.800	0.819	1.168	0.831	0.011	1.135	1.448
2x1	1.330	0.794	92.500	72.100	0.779	-1.831	0.770	0.016	-1.579	-1.258
2x2	2.000	0.853	92.500	78.700	0.851	-0.257	0.849	0.010	-0.477	-0.221
2x3	2.400	0.866	92.500	80.000	0.865	-0.131	0.866	0.010	-0.082	0.165
2x4	2.670	0.873	92.500	80.800	0.874	0.059	0.876	0.010	0.193	0.249
2x5	2.860	0.879	92.500	81.300	0.879	-0.009	0.881	0.009	0.032	0.268
2x7	3.110	0.884	92.500	82.000	0.886	0.281	0.889	0.010	0.148	0.319
2x10	3.330	0.888	92.500	82.400	0.891	0.317	0.896	0.008	0.421	0.555
2x15	3.530	0.890	92.500	82.800	0.895	0.577	0.901	0.007	0.562	0.660
2x20	3.640	0.892	92.500	82.900	0.896	0.473	0.904	0.006	0.772	0.860
2x30	3.750	0.893	92.500	83.200	0.899	0.723	0.907	0.006	0.814	0.874
2x40	3.810	0.893	92.500	83.200	0.899	0.723	0.909	0.006	0.970	1.031
3x1	1.500	0.804	92.500	73.400	0.794	-1.304	0.777	0.018	-2.335	-2.029
3x2	2.400	0.867	92.500	79.900	0.864	-0.371	0.863	0.012	-0.329	-0.074
3x3	3.000	0.896	92.500	82.700	0.894	-0.217	0.886	0.010	-1.132	-0.917
4x1	1.600	0.807	92.500	73.800	0.798	-1.135	0.782	0.018	-2.188	-2.046
4x2	2.670	0.874	92.500	80.600	0.871	-0.303	0.872	0.012	-0.106	0.083
5x1	1.670	0.810	92.500	74.000	0.800	-1.235	0.785	0.019	-2.177	-1.933
5x2	2.860	0.881	92.500	81.100	0.877	-0.482	0.877	0.012	-0.225	0.031
7x1	1.750	0.814	92.500	74.200	0.802	-1.454	0.788	0.020	-1.959	-1.734
7x2	3.110	0.888	92.500	81.600	0.882	-0.657	0.883	0.012	-0.160	0.048
10x1	1.820	0.816	92.500	74.500	0.805	-1.298	0.790	0.021	-2.045	-1.851
10x2	3.330	0.892	92.500	82.000	0.886	-0.618	0.887	0.011	-0.062	0.109
10x10	10.000	1.000	92.500	92.500	1.000	0.000	1.000	0.000	0.000	0.000
15x1	1.880	0.818	92.500	74.600	0.806	-1.408	0.793	0.020	-1.883	-1.698
15x2	3.530	0.896	92.500	82.200	0.889	-0.820	0.892	0.011	0.191	0.343
20x1	1.900	0.819	92.500	74.700	0.808	-1.396	0.794	0.021	-1.884	-1.710
20x2	3.640	0.897	92.500	82.400	0.891	-0.690	0.893	0.010	0.157	0.291
30x1	1.940	0.821	92.500	74.700	0.808	-1.636	0.795	0.021	-1.745	-1.571
30x2	3.750	0.900	92.500	82.500	0.892	-0.901	0.895	0.009	0.263	0.388
40x1	1.950	0.822	92.500	74.800	0.809	-1.624	0.795	0.020	-1.840	-1.676
40x2	3.810	0.900	92.500	82.500	0.892	-0.901	0.896	0.009	0.338	0.463

A.2 MLC OPFs

Table A-5: OPF Measurements using Exradin A16 Micro Ion Chamber (MLCs)

Exradin A16 Measurements MLCs

Field Size (cm)	Reading 1 (nC)	Reading 2 (nC)	Reading 3 (nC)	Avg (nC)	Correction Factor	Corrected Avg (nC)	10x10 Avg (nC)	Measured OPF	Eclipse OPF	% diff
1x1	0.165	0.165	0.165	0.165	1.027	0.169	0.218	0.779	0.772	0.898
1x2	0.174	0.174	0.175	0.174	1.012	0.176	0.218	0.810	0.809	0.217
1x3	0.177	0.177	0.176	0.177	1.008	0.178	0.218	0.819	0.818	0.031
2x1	0.171	0.171	0.171	0.171	1.012	0.173	0.218	0.796	0.801	-0.597
2x2	0.183	0.183	0.183	0.183	1.003	0.184	0.218	0.845	0.864	-2.210
2x3	0.187	0.188	0.187	0.187	1.001	0.187	0.218	0.862	0.879	-1.974
3x1	0.173	0.173	0.174	0.173	1.008	0.175	0.218	0.803	0.809	-0.714
3x2	0.186	0.187	0.187	0.187	1.001	0.187	0.218	0.859	0.878	-2.115
3x3	0.191	0.191	0.191	0.191	1.000	0.191	0.218	0.878	0.897	-2.131
10x10	0.218	0.217	0.218	0.218	1.000	0.218	0.218	1.000	1.000	0.000

Table A-6: OPF Measurements Using Sun Nuclear EDGE Diode Detector (MLCs)

Sun Nuclear EDGE Measurements MLCs

Field Size (cm)	Reading 1 (nC)	Reading 2 (nC)	Reading 3 (nC)	Avg (nC)	Correction Factor	Corrected Avg (nC)	10x10 Avg (nC)	Measured OPF	Eclipse OPF	% diff
1x1	29.720	29.680	29.700	29.700	0.966	28.690	36.970	0.776	0.772	0.537
1x2	30.820	30.730	30.750	30.767	0.981	30.182	36.970	0.816	0.809	0.958
1x3	31.060	31.040	31.110	31.070	0.986	30.635	36.970	0.829	0.818	1.255
2x1	30.440	30.520	30.430	30.463	0.981	29.885	36.970	0.808	0.801	0.907
2x2	31.870	31.880	31.860	31.870	0.994	31.679	36.970	0.857	0.864	-0.799
2x3	32.370	32.360	32.440	32.390	0.997	32.293	36.970	0.873	0.879	-0.618
3x1	30.680	30.670	30.720	30.690	0.986	30.260	36.970	0.819	0.809	1.220
3x2	32.350	32.350	32.300	32.333	0.997	32.236	36.970	0.872	0.878	-0.670
3x3	32.960	32.980	32.960	32.967	0.999	32.934	36.970	0.891	0.897	-0.722
10x10	36.940	36.990	36.980	36.970	1.000	36.970	36.970	1.000	1.000	0.000

Table A-7: OPF Measurements using IBA Razor Diode Detector (MLCs)

IBA Razor Diode Measurements MLCs

Field Size (cm)	Reading 1 (nC)	Reading 2 (nC)	Reading 3 (nC)	Avg (nC)	Correction Factor	Corrected Avg (nC)	10x10 Avg (nC)	Measured OPF	Eclipse OPF	% diff
1x1	3.229	3.227	3.226	3.227	1.007	3.250	4.168	0.780	0.772	1.008
1x2	3.360	3.364	3.364	3.363	1.022	3.437	4.168	0.824	0.809	1.956
1x3	3.402	3.402	3.400	3.401	1.029	3.500	4.168	0.840	0.818	2.600
2x1	3.324	3.332	3.330	3.329	1.022	3.402	4.168	0.816	0.801	1.878
2x2	3.513	3.521	3.519	3.518	1.031	3.627	4.168	0.870	0.864	0.727
2x3	3.580	3.591	3.588	3.586	1.029	3.690	4.168	0.885	0.879	0.729
3x1	3.360	3.361	3.362	3.361	1.031	3.465	4.168	0.831	0.809	2.803
3x2	3.569	3.579	3.572	3.573	1.028	3.673	4.168	0.881	0.878	0.390
3x3	3.660	3.664	3.665	3.663	1.026	3.758	4.168	0.902	0.897	0.481
10x10	4.167	4.167	4.171	4.168	1.000	4.168	4.168	1.000	1.000	0.000

Table A-8: Cumulative OPF Measurementts (MLCs)

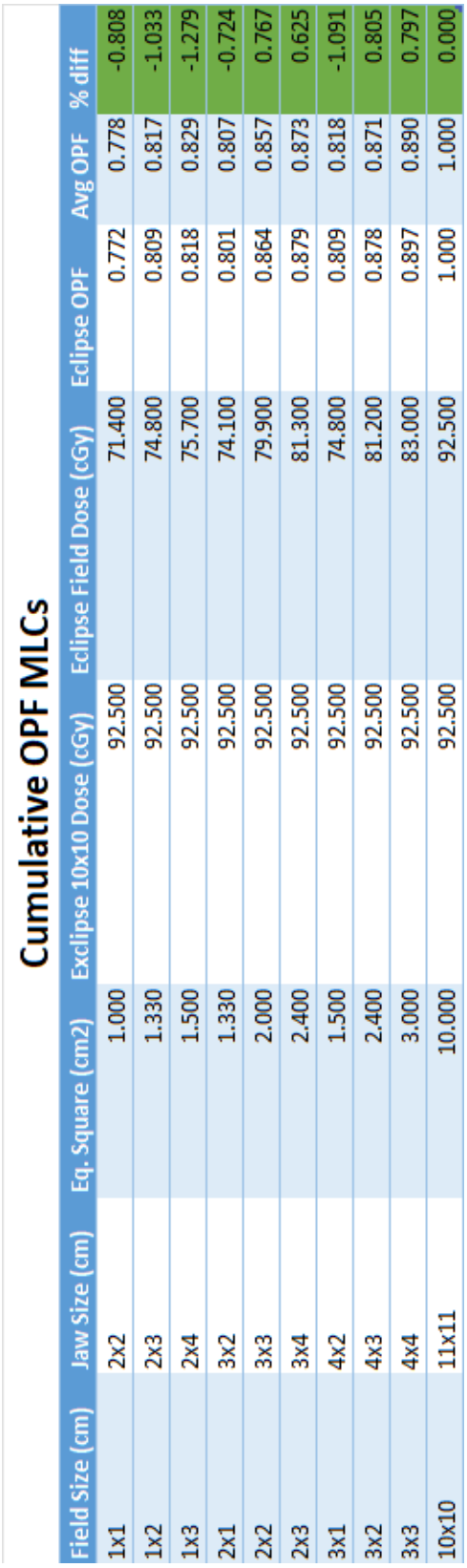

Cumulative OPF MLCs

Field Size (cm)	Jaw Size (cm)	Eq. Square (cm2)	Exclipse 10x10 Dose (cGy)	Eclipse Field Dose (cGy)	Eclipse OPF	Avg OPF	% diff
1x1	2x2	1.000	92.500	71.400	0.772	0.778	-0.808
1x2	2x3	1.330	92.500	74.800	0.809	0.817	-1.033
1x3	2x4	1.500	92.500	75.700	0.818	0.829	-1.279
2x1	3x2	1.330	92.500	74.100	0.801	0.807	-0.724
2x2	3x3	2.000	92.500	79.900	0.864	0.857	0.767
2x3	3x4	2.400	92.500	81.300	0.879	0.873	0.625
3x1	4x2	1.500	92.500	74.800	0.809	0.818	-1.091
3x2	4x3	2.400	92.500	81.200	0.878	0.871	0.805
3x3	4x4	3.000	92.500	83.000	0.897	0.890	0.797
10x10	11x11	10.000	92.500	92.500	1.000	1.000	0.000

APPENDIX B. RETROSPECTIVE ANALYSIS DATA

B.1 Clear Checks

Priority	Structure Template	Structure Plan	Type	Prescription	Constraint	Goal	MultiSiteSRS	AXBe 13100	Difference	Pass/Fail
1	PTV_1	PTV_LtFrontal	Target	**Total Dose: 1400cGy**	V100% ≥	95%	100%	100%	0	✓
2	PTV_1	PTV_LtFrontal	Target	**Total Dose: 1400cGy**	V95% ≥	100%	100%	100%	0	✓
3	PTV_1	PTV_LtFrontal	Target	**Total Dose: 1400cGy**	D0.035cc ≤ (HI)	130%	127.19%	127.193%	-0.003	✓
4	PTV_1	PTV_LtFrontal	Target	**Total Dose: 1400cGy**	**CI using PTV_LtFrontal 100%**	1.2-1.5	1.306	1.288	0.018	AXBe 13100
5	PTV_2	PTV_LtParietal	Target	**Total Dose: 1400cGy**	V100% ≥	95%	99.93%	99.931%	-0.001	✓
6	PTV_2	PTV_LtParietal	Target	**Total Dose: 1400cGy**	V95% ≥	100%	100%	100%	0	✓
7	PTV_2	PTV_LtParietal	Target	**Total Dose: 1400cGy**	D0.035cc ≤ (HI)	130%	127.909%	127.804%	0.105	✓
8	PTV_2	PTV_LtParietal	Target	**Total Dose: 1400cGy**	**CI using PTV_LtParietal 100%**	1.2-1.5	1.379	1.365	0.014	AXBe 13100
9	PTV_3	PTV_RtFrontal	Target	**Total Dose: 1400cGy**	V100% ≥	95%	99.616%	99.907%	-0.291	✓
10	PTV_3	PTV_RtFrontal	Target	**Total Dose: 1400cGy**	V95% ≥	100%	100%	100%	0	✓
11	PTV_3	PTV_RtFrontal	Target	**Total Dose: 1400cGy**	D0.035cc ≤ (HI)	130%	128.444%	128.328%	0.116	✓
12	PTV_3	PTV_RtFrontal	Target	**Total Dose: 1400cGy**	**CI using PTV_RtFrontal 100%**	1.2-1.5	1.265	1.251	0.014	AXBe 13100
13	Brainstem	BrainStem	OAR		D0.035cc ≤	1500cGy	150.5cGy	151.1cGy	-0.6	✓
14	Brainstem	BrainStem	OAR		D0.5cc ≤	1000cGy	132.3cGy	132.9cGy	-0.6	✓
15	Chiasm	Chiasm	OAR		D0.035cc ≤	1000cGy	52.3cGy	52.5cGy	-0.2	✓
16	Cochlea_L	Cochlea_L	OAR		Max ≤	900cGy	26.2cGy	26.4cGy	-0.2	✓
17	Cochlea_L	Cochlea_L	OAR		Mean ≤ (Optimal)	400cGy	21.9cGy	22.6cGy	-0.7	✓
18	Cochlea_L	Cochlea_L	OAR		Mean ≤ (Mandatory)	900cGy	21.9cGy	22.6cGy	-0.7	✓
19	Cochlea_R	Cochlea_R	OAR		Max ≤	900cGy	29.3cGy	24cGy	5.3	✓
20	Cochlea_R	Cochlea_R	OAR		Mean ≤ (Optimal)	400cGy	25.3cGy	23cGy	2.3	✓
21	Cochlea_R	Cochlea_R	OAR		Mean ≤ (Mandatory)	900cGy	25.3cGy	23cGy	2.3	✓
22	Eye_L	Eye_L	OAR		D0.035cc ≤	500cGy	71.5cGy	70cGy	1.5	✓
23	Eye_R	Eye_R	OAR		D0.035cc ≤	500cGy	45.5cGy	40.3cGy	5.2	✓

Figure B-1: Clear Check Case 13100

Priority	Structure Template	Structure Plan	Type	Prescription	Constraint	Goal	SRS MultiMets	AXBe 13125	Difference	Pass/Fail
1	**PTV1**	PTV_1 (21Gy)	Target	**21Gy: 2100cGy**	V100% ≥	95%	98.516%	98.354%	0.162	✓
2	**PTV1**	PTV_1 (21Gy)	Target	**21Gy: 2100cGy**	V95% ≥	100%	100%	100%	0	✓
3	**PTV1**	PTV_1 (21Gy)	Target	**21Gy: 2100cGy**	D0.035cc ≤ (HI)	130%	125.946%	125.99%	-0.044	✓
4	**PTV2**	**PTV_2 (21Gy)**	**Target**	**21Gy: 2100cGy**	**V100% ≥**	**95%**	99.706%	99.609%	0.097	✓
5	**PTV2**	**PTV_2 (21Gy)**	**Target**	**21Gy: 2100cGy**	**V95% ≥**	**100%**	100%	100%	0	✓
6	**PTV2**	**PTV_2 (21Gy)**	**Target**	**21Gy: 2100cGy**	**D0.035cc ≤ (HI)**	**130%**	126.331%	126.219%	0.112	✓
7	**PTV3**	**PTV_3 (20Gy)**	**Target**	**20Gy: 2000cGy**	**V100% ≥**	**95%**	99.782%	99.222%	0.56	✓
8	**PTV3**	**PTV_3 (20Gy)**	**Target**	**20Gy: 2000cGy**	**V95% ≥**	**100%**	100%	99.997%	0.003	SRS MultiMets
9	**PTV3**	**PTV_3 (20Gy)**	**Target**	**20Gy: 2000cGy**	**D0.035cc ≤ (HI)**	**130%**	120.557%	119.401%	1.156	✓
10	**PTV4**	**PTV_4 (20Gy)**	**Target**	**20Gy: 2000cGy**	**V100% ≥**	**95%**	99.908%	100%	-0.092	✓
11	**PTV4**	**PTV_4 (20Gy)**	**Target**	**20Gy: 2000cGy**	**V95% ≥**	**100%**	100%	100%	0	✓
12	**PTV4**	**PTV_4 (20Gy)**	**Target**	**20Gy: 2000cGy**	**D0.035cc ≤ (HI)**	**130%**	122.385%	122.415%	-0.03	✓
13	Brainstem	BrainStem	OAR		D0.035cc ≤	1500cGy	259.5cGy	260.1cGy	-0.6	✓
14	Brainstem	BrainStem	OAR		D0.5cc ≤	1000cGy	218.1cGy	219cGy	-0.9	✓
15	Chiasm	Chiasm	OAR		D0.035cc ≤	1000cGy	99.4cGy	95.3cGy	4.1	✓
16	Cochlea_L	Cochlea_L	OAR		Max ≤	900cGy	162.5cGy	164.8cGy	-2.3	✓
17	Cochlea_R	Cochlea_R	OAR		Max ≤	900cGy	84.7cGy	83.1cGy	1.6	✓
18	Eye_L	Eye_L	OAR		D0.035cc ≤	500cGy	40.4cGy	35.9cGy	4.5	✓
19	Eye_R	Eye_R	OAR		D0.035cc ≤	500cGy	31.3cGy	32.2cGy	-0.9	✓
20	Lens_L	Lens_L	OAR		D0.035cc ≤	100cGy	18cGy	16.6cGy	1.4	✓
21	Lens_R	Lens_R	OAR		D0.035cc ≤	100cGy	15.2cGy	18cGy	-2.8	✓
22	OpticNerve_L	OpticNerve_L	OAR		D0.035cc ≤	1000cGy	109.3cGy	110.8cGy	-1.5	✓
23	OpticNerve_R	OpticNerve_R	OAR		D0.035cc ≤	1000cGy	125.6cGy	124.9cGy	0.7	✓
24	OpticTract_Lt	OpticTract_Lt	OAR		D0.035cc ≤	1000cGy	89.6cGy	88.6cGy	1	✓
25	OpticTract_Rt	OpticTract_Rt	OAR		D0.035cc ≤	1000cGy	157cGy	144.1cGy	12.9	✓
26	Brain-PTV	Brain-PTV	OAR		V1200cGy ≤	10cc	14.084cc	14.125cc	-0.041	SRS MultiMets

Figure B-2: Clear Check case 13125

Priority	Structure Template	Structure Plan	Type	Prescription	Constraint	Goal	SRS MultiMets	AXBe 41080	Difference	Pass/Fail
1	**PTV_Lt Parietal**	PTV_Lt Parietal	Target	Total Dose: 2100cGy	V100% ≥	95%	99.988%	99.995%	-0.007	✓
2	**PTV_Lt Parietal**	PTV_Lt Parietal	Target	Total Dose: 2100cGy	V95% ≥	100%	100%	100%	0	✓
3	**PTV_Lt Parietal**	PTV_Lt Parietal	Target	Total Dose: 2100cGy	D0.035cc ≤ (HI)	130%	128.007%	127.872%	0.135	✓
4	**PTV_Rt Front Para**	**PTV_R Front Parasag**	**Target**	**Total Dose: 2100cGy**	**V100% ≥**	**95%**	99.688%	99.892%	-0.204	✓
5	**PTV_Rt Front Para**	**PTV_R Front Parasag**	**Target**	**Total Dose: 2100cGy**	**V95% ≥**	**100%**	100%	100%	0	✓
6	**PTV_Rt Front Para**	**PTV_R Front Parasag**	**Target**	**Total Dose: 2100cGy**	**D0.035cc ≤ (HI)**	**130%**	128.072%	127.959%	0.113	✓
7	**PTV_Rt Occipital**	**PTV_Rt Occipital**	**Target**	**Total Dose: 2100cGy**	**V100% ≥**	**95%**	99.831%	100%	-0.169	✓
8	**PTV_Rt Occipital**	**PTV_Rt Occipital**	**Target**	**Total Dose: 2100cGy**	**V95% ≥**	**100%**	100%	100%	0	✓
9	**PTV_Rt Occipital**	**PTV_Rt Occipital**	**Target**	**Total Dose: 2100cGy**	**D0.035cc ≤ (HI)**	**130%**	127.177%	127.044%	0.133	✓
10	**PTV_Rt Supinsular**	**PTV_Rt Subinsular**	**Target**	**Total Dose: 2100cGy**	**V100% ≥**	**95%**	99.984%	99.7%	0.284	✓
11	**PTV_Rt Supinsular**	**PTV_Rt Subinsular**	**Target**	**Total Dose: 2100cGy**	**V95% ≥**	**100%**	100%	100%	0	✓
12	**PTV_Rt Supinsular**	**PTV_Rt Subinsular**	**Target**	**Total Dose: 2100cGy**	**D0.035cc ≤ (HI)**	**130%**	127.9%	127.658%	0.242	✓
13	**PTV_Rt Temporal**	**PTV_Rt Temporal**	**Target**	**Total Dose: 2100cGy**	**V100% ≥**	**95%**	100%	100%	0	✓
14	**PTV_Rt Temporal**	**PTV_Rt Temporal**	**Target**	**Total Dose: 2100cGy**	**V95% ≥**	**100%**	100%	100%	0	✓
15	**PTV_Rt Temporal**	**PTV_Rt Temporal**	**Target**	**Total Dose: 2100cGy**	**D0.035cc ≤ (HI)**	**130%**	126.565%	127.056%	-0.491	✓
16	Brainstem	BrainStem	OAR		D0.035cc ≤	1500cGy	536.4cGy	530.8cGy	5.6	✓
17	Brainstem	BrainStem	OAR		D0.5cc ≤	1000cGy	435.6cGy	434.7cGy	0.9	✓
18	Chiasm	Chiasm	OAR		D0.035cc ≤	1000cGy	228.3cGy	230.5cGy	-2.2	✓
19	Cochlea_L	Cochlea_L	OAR		Max ≤	900cGy	78cGy	79.7cGy	-1.7	✓
20	Cochlea_R	Cochlea_R	OAR		Max ≤	900cGy	199.2cGy	197.3cGy	1.9	✓
21	Eye_L	Eye_L	OAR		D0.035cc ≤	500cGy	74.6cGy	87.9cGy	-13.3	✓
22	Eye_R	Eye_R	OAR		D0.035cc ≤	500cGy	138.2cGy	138.3cGy	-0.1	✓
23	Lens_L	Lens_L	OAR		D0.035cc ≤	100cGy	62.9cGy	60.5cGy	2.4	✓
24	Lens_R	Lens_R	OAR		D0.035cc ≤	100cGy	83.1cGy	81.9cGy	1.2	✓

Figure B-3: Clear Check case 41080

Priority	Structure Template	Structure Plan	Type	Prescription	Constraint	Goal	17656	AXBe 17656	Difference	Pass/Fail
1	PTV_1	PTV_Rt_Occipital_21Gy	Target	**Total Dose: 2100cGy**	V100% ≥	95%	100%	100%	0	✓
2	PTV_1	PTV_Rt_Occipital_21Gy	Target	**Total Dose: 2100cGy**	V95% ≥	100%	100%	100%	0	✓
3	PTV_1	PTV_Rt_Occipital_21Gy	Target	**Total Dose: 2100cGy**	D0.035cc ≤ (HI)	130%	122.151%	121.675%	0.476	✓
4	PTV_1	PTV_Rt_Occipital_21Gy	Target	**Total Dose: 2100cGy**	**CI using PTV_Rt_Occipital_21**	1.2-1.5	1.866	1.853	0.013	AXBe 17656
5	PTV_2	PTV_Lt_FrontoParietal_21Gy	Target	**Total Dose: 2100cGy**	V100% ≥	95%	99.9%	99.9%	0	✓
6	PTV_2	PTV_Lt_FrontoParietal_21Gy	Target	**Total Dose: 2100cGy**	V95% ≥	100%	100%	100%	0	✓
7	PTV_2	PTV_Lt_FrontoParietal_21Gy	Target	**Total Dose: 2100cGy**	D0.035cc ≤ (HI)	130%	127.043%	127.685%	-0.642	✓
8	PTV_2	PTV_Lt_FrontoParietal_21Gy	Target	**Total Dose: 2100cGy**	**CI using PTV_Lt_FrontoParietal**	1.2-1.5	1.315	1.302	0.013	△
9	PTV_3	PTV_Lt_Occipital_21Gy	Target	**Total Dose: 2100cGy**	V100% ≥	95%	99.618%	99.617%	0.001	✓
10	PTV_3	PTV_Lt_Occipital_21Gy	Target	**Total Dose: 2100cGy**	V95% ≥	100%	100%	100%	0	✓
11	PTV_3	PTV_Lt_Occipital_21Gy	Target	**Total Dose: 2100cGy**	D0.035cc ≤ (HI)	130%	127.076%	127.422%	-0.346	✓
12	PTV_3	PTV_Lt_Occipital_21Gy	Target	**Total Dose: 2100cGy**	**CI using PTV_Lt_Occipital_21**	1.2-1.5	1.272	1.261	0.011	△
21	Brainstem	BrainStem	OAR		D0.035cc ≤	1500cGy	169.2cGy	167.5cGy	1.7	✓
22	Brainstem	BrainStem	OAR		D0.5cc ≤	1000cGy	152.1cGy	148.2cGy	3.9	✓
23	Chiasm	Chiasm	OAR		D0.035cc ≤	1000cGy	132.5cGy	133.6cGy	-1.1	✓
24	Cochlea_L	Cochlea_L	OAR		Max ≤	900cGy	72.4cGy	88.3cGy	-15.9	✓
25	Cochlea_L	Cochlea_L	OAR		Mean ≤ (Optimal)	400cGy	67.9cGy	61.3cGy	6.6	✓
26	Cochlea_L	Cochlea_L	OAR		Mean ≤ (Mandatory)	900cGy	67.9cGy	61.3cGy	6.6	✓
27	Cochlea_R	Cochlea_R	OAR		Max ≤	900cGy	84.8cGy	61.5cGy	23.3	✓
28	Cochlea_R	Cochlea_R	OAR		Mean ≤ (Optimal)	400cGy	80.2cGy	56.3cGy	23.9	✓
29	Cochlea_R	Cochlea_R	OAR		Mean ≤ (Mandatory)	900cGy	80.2cGy	56.3cGy	23.9	✓
30	Eye_L	Eye_L	OAR		D0.035cc ≤	500cGy	65.3cGy	67.2cGy	-1.9	✓
31	Eye_R	Eye_R	OAR		D0.035cc ≤	500cGy	20.7cGy	46.6cGy	-25.9	✓

Figure B-4: Clear Check case 17656

Priority	Structure Template	Structure Plan	Type	Prescription	Constraint	Goal	89942	AXBe 89942	Difference	Pass/Fail
1	PTV_1	PTV_Rt Occipital	Target	**Total Dose: 2200cGy**	V100% ≥	95%	100%	100%	0	✓
2	PTV_1	PTV_Rt Occipital	Target	**Total Dose: 2200cGy**	V95% ≥	100%	100%	100%	0	✓
3	PTV_1	PTV_Rt Occipital	Target	**Total Dose: 2200cGy**	D0.035cc ≤ (HI)	130%	129.871%	129.728%	0.143	✓
4	PTV_1	PTV_Rt Occipital	Target	**Total Dose: 2200cGy**	**CI using PTV_Rt Occipital 100**	1.2-1.5	1.158	1.147	0.011	✓
5	PTV_2	PTV_Rt Sup Cerebellum	Target	**Total Dose: 2200cGy**	V100% ≥	95%	100%	100%	0	✓
6	PTV_2	PTV_Rt Sup Cerebellum	Target	**Total Dose: 2200cGy**	V95% ≥	100%	100%	100%	0	✓
7	PTV_2	PTV_Rt Sup Cerebellum	Target	**Total Dose: 2200cGy**	D0.035cc ≤ (HI)	130%	126.366%	125.513%	0.853	✓
8	PTV_2	PTV_Rt Sup Cerebellum	Target	**Total Dose: 2200cGy**	**CI using PTV_Rt Sup Cerebell**	1.2-1.5	1.467	1.385	0.082	△
9	Brainstem	BrainStem	OAR		D0.035cc ≤	1500cGy	244cGy	242.9cGy	1.1	✓
10	Brainstem	BrainStem	OAR		D0.5cc ≤	1000cGy	211.5cGy	210.6cGy	0.9	✓
11	Chiasm	Chiasm	OAR		D0.035cc ≤	1000cGy	91.7cGy	85.7cGy	6	✓
12	Cochlea_L	Cochlea_L	OAR		Max ≤	900cGy	56cGy	60.6cGy	-4.6	✓
13	Cochlea_L	Cochlea_L	OAR		Mean ≤ (Optimal)	400cGy	44.8cGy	48.4cGy	-3.6	✓
14	Cochlea_L	Cochlea_L	OAR		Mean ≤ (Mandatory)	900cGy	44.8cGy	48.4cGy	-3.6	✓
15	Cochlea_R	Cochlea_R	OAR		Max ≤	900cGy	107.4cGy	122.3cGy	-14.9	✓
16	Cochlea_R	Cochlea_R	OAR		Mean ≤ (Optimal)	400cGy	85.2cGy	92.9cGy	-7.7	✓
17	Cochlea_R	Cochlea_R	OAR		Mean ≤ (Mandatory)	900cGy	85.2cGy	92.9cGy	-7.7	✓
18	Eye_L	Eye_L	OAR		D0.035cc ≤	500cGy	32.7cGy	36.4cGy	-3.7	✓
19	Eye_R	Eye_R	OAR		D0.035cc ≤	500cGy	31.1cGy	30.9cGy	0.2	✓
20	Lens_L	Lens_L	OAR		D0.035cc ≤	100cGy	N/A	N/A		
21	Lens_R	Lens_R	OAR		D0.035cc ≤	100cGy	N/A	N/A		
22	OpticNerve_L	OpticNerve_L	OAR		D0.035cc ≤	1000cGy	53.2cGy	58.2cGy	-5	✓
23	OpticNerve_R	OpticNerve_R	OAR		D0.035cc ≤	1000cGy	71.3cGy	71.4cGy	-0.1	✓
24	OpticTract_Lt	OpticTract_Lt	OAR		D0.035cc ≤	1000cGy	62.5cGy	67.9cGy	-5.4	✓
25	OpticTract_Rt	OpticTract_Rt	OAR		D0.035cc ≤	1000cGy	127.6cGy	110cGy	17.6	✓
26	Brain-PTV	Brain-PTV	OAR		V1200cGy ≤	10cc	9.424cc	9.418cc	0.006	✓

Figure B-5: Clear Check case 88942

Priority	Structure Template	Structure Plan	Type	Prescription	Constraint	Goal	38946	AXBe 38946	Difference	Pass/Fail
1	PTV_1	PTV_L Post Med Frontal	Target	**Total Dose: 2100cGy**	V100% ≥	95%	100%	100%	0	✓
2	PTV_1	PTV_L Post Med Frontal	Target	**Total Dose: 2100cGy**	V95% ≥	100%	100%	100%	0	✓
3	PTV_1	PTV_L Post Med Frontal	Target	**Total Dose: 2100cGy**	D0.035cc ≤ (HI)	130%	125.086%	123.509%	1.577	✓
4	PTV_1	PTV_L Post Med Frontal	Target	**Total Dose: 2100cGy**	**CI using PTV_L Post Med Fron**	1.2-1.5	1.367	1.254	0.113	△
5	Brainstem	BrainStem	OAR		D0.035cc ≤	1500cGy	47.3cGy	49.7cGy	-2.4	✓
6	Brainstem	BrainStem	OAR		D0.5cc ≤	1000cGy	41cGy	41.2cGy	-0.2	✓
7	Chiasm	Chiasm	OAR		D0.035cc ≤	1000cGy	13.2cGy	14.3cGy	-1.1	✓
8	Cochlea_L	Cochlea_L	OAR		Max ≤	900cGy	3.1cGy	3.3cGy	-0.2	✓
9	Cochlea_L	Cochlea_L	OAR		Mean ≤ (Optimal)	400cGy	2.6cGy	3cGy	-0.4	✓
10	Cochlea_L	Cochlea_L	OAR		Mean ≤ (Mandatory)	900cGy	2.6cGy	3cGy	-0.4	✓
11	Cochlea_R	Cochlea_R	OAR		Max ≤	900cGy	2.6cGy	3.4cGy	-0.8	✓
12	Cochlea_R	Cochlea_R	OAR		Mean ≤ (Optimal)	400cGy	2.1cGy	3cGy	-0.9	✓
13	Cochlea_R	Cochlea_R	OAR		Mean ≤ (Mandatory)	900cGy	2.1cGy	3cGy	-0.9	✓
14	Eye_L	Eye_L	OAR		D0.035cc ≤	500cGy	8.7cGy	7cGy	1.7	✓
15	Eye_R	Eye_R	OAR		D0.035cc ≤	500cGy	18.3cGy	15.1cGy	3.2	✓
16	Lens_L	Lens_L	OAR		D0.035cc ≤	100cGy	2.4cGy	2.8cGy	-0.4	✓
17	Lens_R	Lens_R	OAR		D0.035cc ≤	100cGy	10.5cGy	9.6cGy	0.9	✓
18	OpticNerve_L	OpticNerve_L	OAR		D0.035cc ≤	1000cGy	19.3cGy	17.1cGy	2.2	✓
19	OpticNerve_R	OpticNerve_R	OAR		D0.035cc ≤	1000cGy	11.7cGy	11.4cGy	0.3	✓
20	OpticTract_Lt	OpticTract_Lt	OAR		D0.035cc ≤	1000cGy	26.4cGy	22.5cGy	3.9	✓
21	OpticTract_Rt	OpticTract_Rt	OAR		D0.035cc ≤	1000cGy	6.5cGy	8.6cGy	-2.1	✓
22	Brain-PTV	Brain-PTV	OAR		V1200cGy ≤	10cc	2.343cc	2.305cc	0.038	✓
23	Brain-PTV	Brain-PTV	OAR		V500cGy ≤	50%	0.658%	0.646%	0.012	✓

Figure B-6: Clear Check case 38946

Priority	Structure Template	Structure Plan	Type	Prescription	Constraint	Goal	59758	AXBe 59758	Difference	Pass/Fail
1	PTV_1	PTV_It post frontal	Target	**Total Dose: 2100cGy**	V100% ≥	95%	100%	100%	0	✓
2	PTV_1	PTV_It post frontal	Target	**Total Dose: 2100cGy**	V95% ≥	100%	100%	100%	0	✓
3	PTV_1	PTV_It post frontal	Target	**Total Dose: 2100cGy**	D0.035cc ≤ (HI)	130%	124.314%	124.126%	0.188	✓
4	PTV_1	PTV_It post frontal	Target	**Total Dose: 2100cGy**	**CI using PTV_It post frontal 1**	1.2-1.5	1.362	1.341	0.021	△
5	Brainstem	BrainStem	OAR		D0.035cc ≤	1500cGy	39.7cGy	48.2cGy	-8.5	✓
6	Brainstem	BrainStem	OAR		D0.5cc ≤	1000cGy	32.1cGy	34.6cGy	-2.5	✓
7	Chiasm	Chiasm	OAR		D0.035cc ≤	1000cGy	33.3cGy	28.8cGy	4.5	✓
8	Cochlea_L	Cochlea_L	OAR		Max ≤	900cGy	12.1cGy	11.4cGy	0.7	✓
9	Cochlea_L	Cochlea_L	OAR		Mean ≤ (Optimal)	400cGy	11.1cGy	10.7cGy	0.4	✓
10	Cochlea_L	Cochlea_L	OAR		Mean ≤ (Mandatory)	900cGy	11.1cGy	10.7cGy	0.4	✓
11	Cochlea_R	Cochlea_R	OAR		Max ≤	900cGy	10.1cGy	9.4cGy	0.7	✓
12	Cochlea_R	Cochlea_R	OAR		Mean ≤ (Optimal)	400cGy	7cGy	8.3cGy	-1.3	✓
13	Cochlea_R	Cochlea_R	OAR		Mean ≤ (Mandatory)	900cGy	7cGy	8.3cGy	-1.3	✓
14	Eye_L	Eye_L	OAR		D0.035cc ≤	500cGy	6.8cGy	5.7cGy	1.1	✓
15	Eye_R	Eye_R	OAR		D0.035cc ≤	500cGy	20.6cGy	20.2cGy	0.4	✓
16	Lens_L	Lens_L	OAR		D0.035cc ≤	100cGy	N/A	N/A		
17	Lens_R	Lens_R	OAR		D0.035cc ≤	100cGy	N/A	N/A		
18	OpticNerve_L	OpticNerve_L	OAR		D0.035cc ≤	1000cGy	5.8cGy	5.7cGy	0.1	✓
19	OpticNerve_R	OpticNerve_R	OAR		D0.035cc ≤	1000cGy	30.7cGy	28.4cGy	2.3	✓
20	OpticTract_Lt	OpticTract_Lt	OAR		D0.035cc ≤	1000cGy	8.5cGy	18.8cGy	-10.3	✓
21	OpticTract_Rt	OpticTract_Rt	OAR		D0.035cc ≤	1000cGy	48.3cGy	49.2cGy	-0.9	✓
22	Brain-PTV	Brain-PTV	OAR		V1200cGy ≤	10cc	2.876cc	2.896cc	-0.02	✓
23	Brain-PTV	Brain-PTV	OAR		V500cGy ≤	50%	0.926%	0.93%	-0.004	✓

Figure B-7: Clear Check case 59758

Priority	Structure Template	Structure Plan	Type	Prescription	Constraint	Goal	20063	AXBe 20063	Difference	Pass/Fail
1	PTV_1	PTV_Rt Inf Cerebellum	Target	**Total Dose: 2100cGy**	V100% ≥	95%	99.97%	98.615%	1.355	✓
2	PTV_1	PTV_Rt Inf Cerebellum	Target	**Total Dose: 2100cGy**	V95% ≥	100%	100%	100%	0	✓
3	PTV_1	PTV_Rt Inf Cerebellum	Target	**Total Dose: 2100cGy**	D0.035cc ≤ (HI)	130%	125.5%	121.946%	3.554	✓
4	PTV_1	PTV_Rt Inf Cerebellum	Target	**Total Dose: 2100cGy**	**CI using PTV_Rt Inf Cerebellu**	1.2-1.5	1.329	1.119	0.21	AXBe 20063
13	Brainstem	BrainStem	OAR		D0.035cc ≤	1500cGy	144.3cGy	143.7cGy	0.6	✓
14	Brainstem	BrainStem	OAR		D0.5cc ≤	1000cGy	121.3cGy	118.2cGy	3.1	✓
15	Chiasm	Chiasm	OAR		D0.035cc ≤	1000cGy	3.8cGy	4.6cGy	-0.8	✓
16	Cochlea_L	Cochlea_L	OAR		Max ≤	900cGy	4.6cGy	3.5cGy	1.1	✓
17	Cochlea_L	Cochlea_L	OAR		Mean ≤ (Optimal)	400cGy	4.3cGy	3.2cGy	1.1	✓
18	Cochlea_L	Cochlea_L	OAR		Mean ≤ (Mandatory)	900cGy	4.3cGy	3.2cGy	1.1	✓
19	Cochlea_R	Cochlea_R	OAR		Max ≤	900cGy	22.1cGy	33.8cGy	-11.7	✓
20	Cochlea_R	Cochlea_R	OAR		Mean ≤ (Optimal)	400cGy	16.4cGy	22.2cGy	-5.8	✓
21	Cochlea_R	Cochlea_R	OAR		Mean ≤ (Mandatory)	900cGy	16.4cGy	22.2cGy	-5.8	✓
22	Eye_L	Eye_L	OAR		D0.035cc ≤	500cGy	5.7cGy	7.8cGy	-2.1	✓
23	Eye_R	Eye_R	OAR		D0.035cc ≤	500cGy	3.7cGy	3.9cGy	-0.2	✓
24	Lens_L	Lens_L	OAR		D0.035cc ≤	100cGy	N/A	N/A		
25	Lens_R	Lens_R	OAR		D0.035cc ≤	100cGy	N/A	N/A		
26	OpticNerve_L	OpticNerve_L	OAR		D0.035cc ≤	1000cGy	19.6cGy	21.7cGy	-2.1	✓
27	OpticNerve_R	OpticNerve_R	OAR		D0.035cc ≤	1000cGy	3.6cGy	4.4cGy	-0.8	✓
28	OpticTract_Lt	OpticTract_Lt	OAR		D0.035cc ≤	1000cGy	4.5cGy	13.6cGy	-9.1	✓
29	OpticTract_Rt	OpticTract_Rt	OAR		D0.035cc ≤	1000cGy	4.6cGy	6.9cGy	-2.3	✓
30	Brain-PTV	Brain-PTV	OAR		V1200cGy ≤	10cc	2.039cc	1.925cc	0.114	✓
31	Brain-PTV	Brain-PTV	OAR		V500cGy ≤	50%	0.569%	0.549%	0.02	✓

Figure B-8: Clear Check case 20063

B.2 SRS MapCheck QA

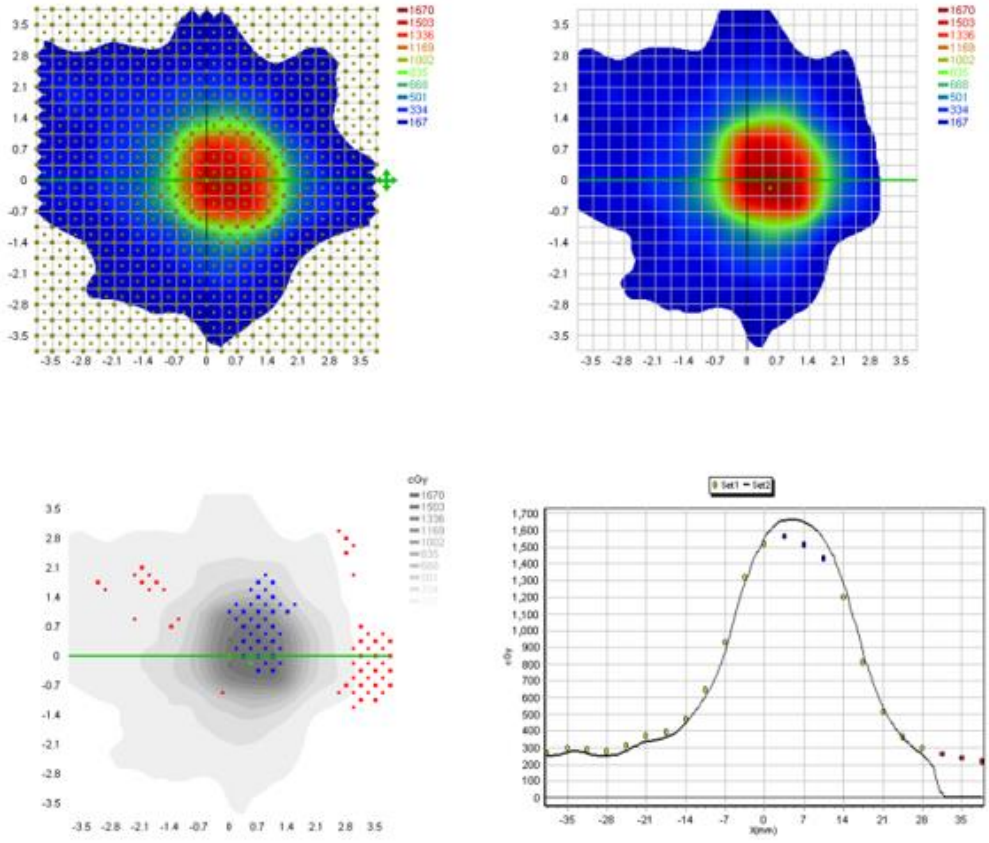

Pass (%)	86.4
Pass	579
Fail	91
Total Points	670

Figure B-9: SRS Mapcheck QA case 13100 original plan

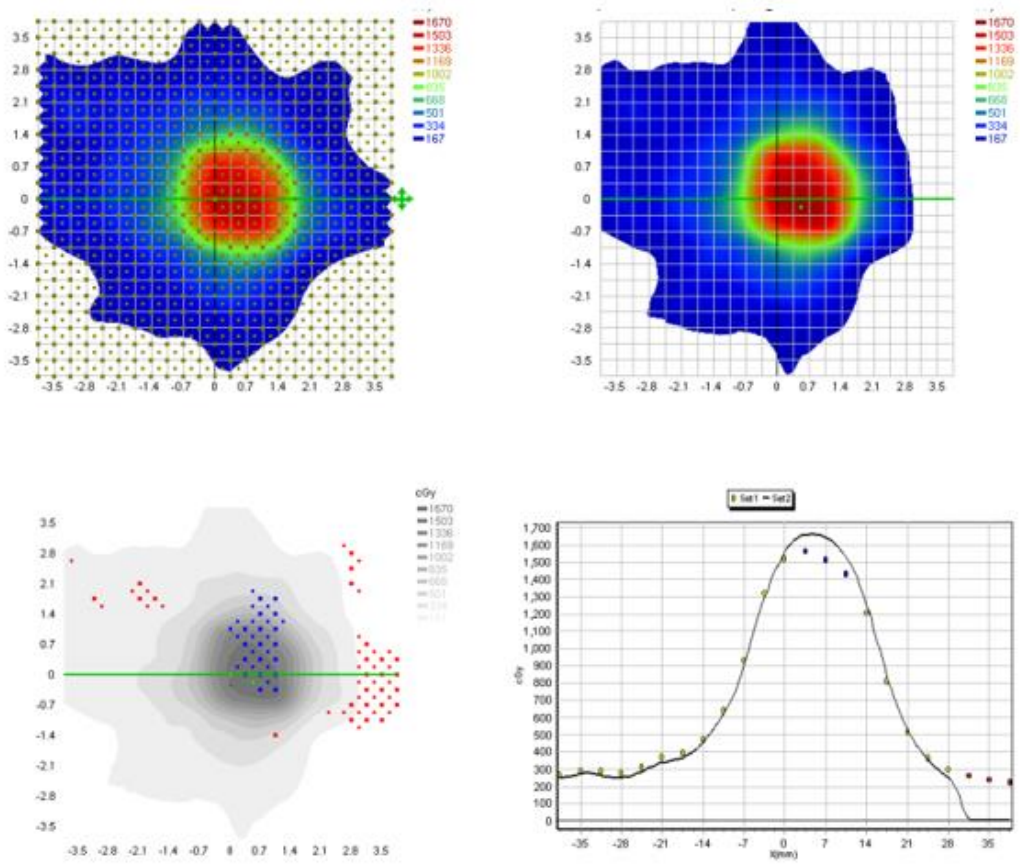

Pass (%)	86.7
Pass	582
Fail	89
Total Points	671

Figure B-10: SRS Mapcheck QA case 13100 AXBe plan

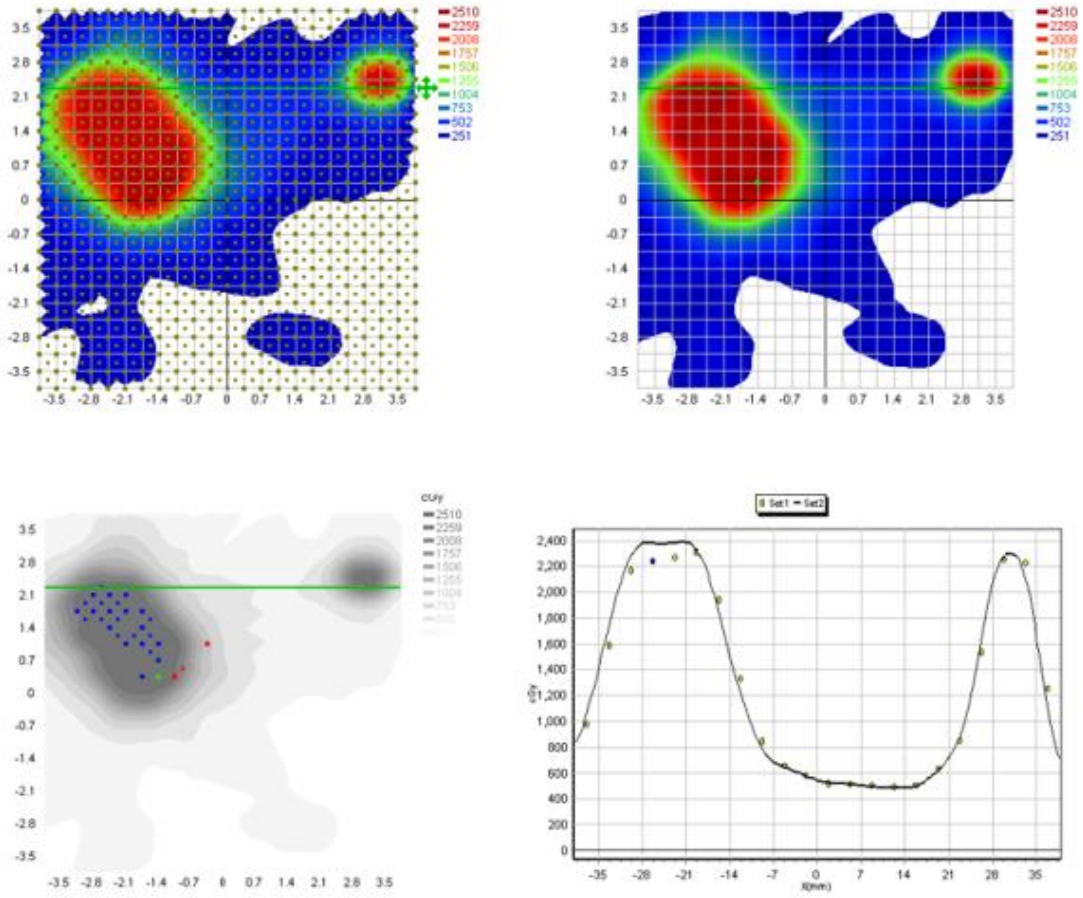

Figure B-11: SRS Mapcheck QA case 13125 original plan

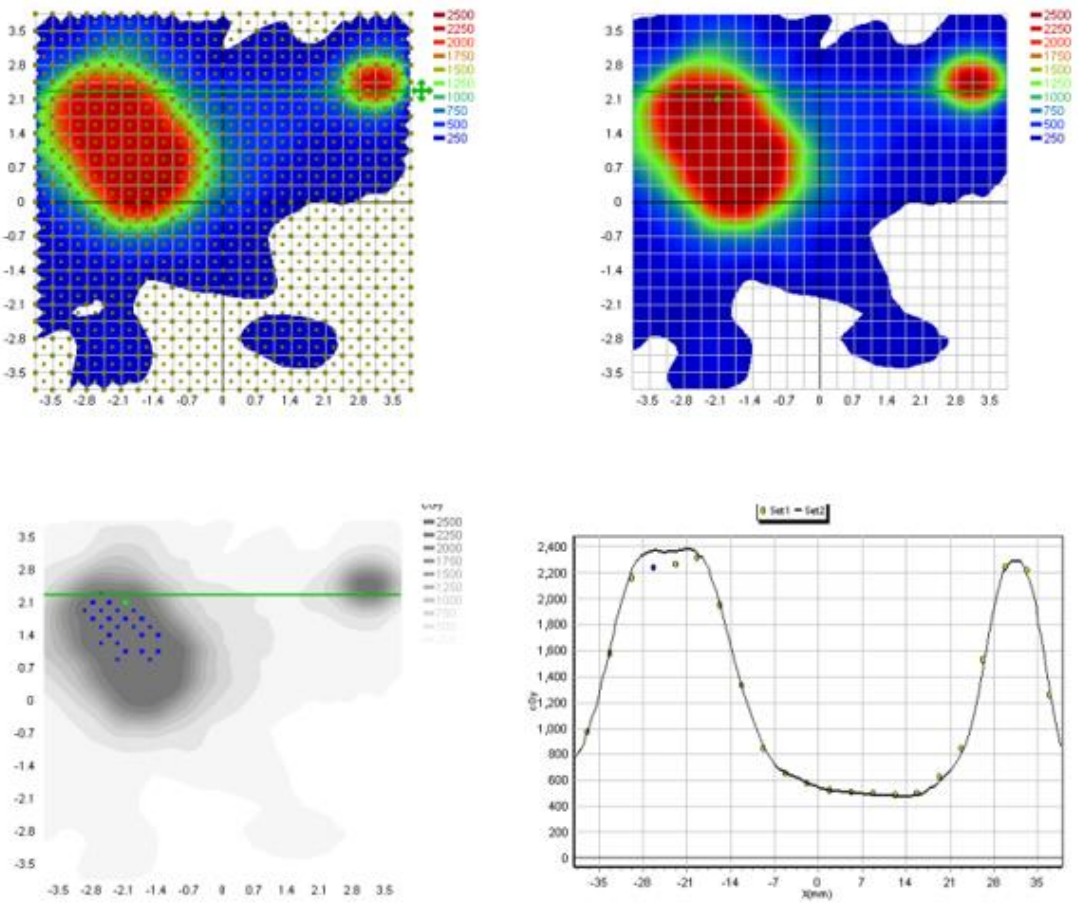

Pass (%)	96.5
Pass	723
Fail	26
Total Points	749

Figure B-12: SRS Mapcheck QA case 13125 AXBe plan

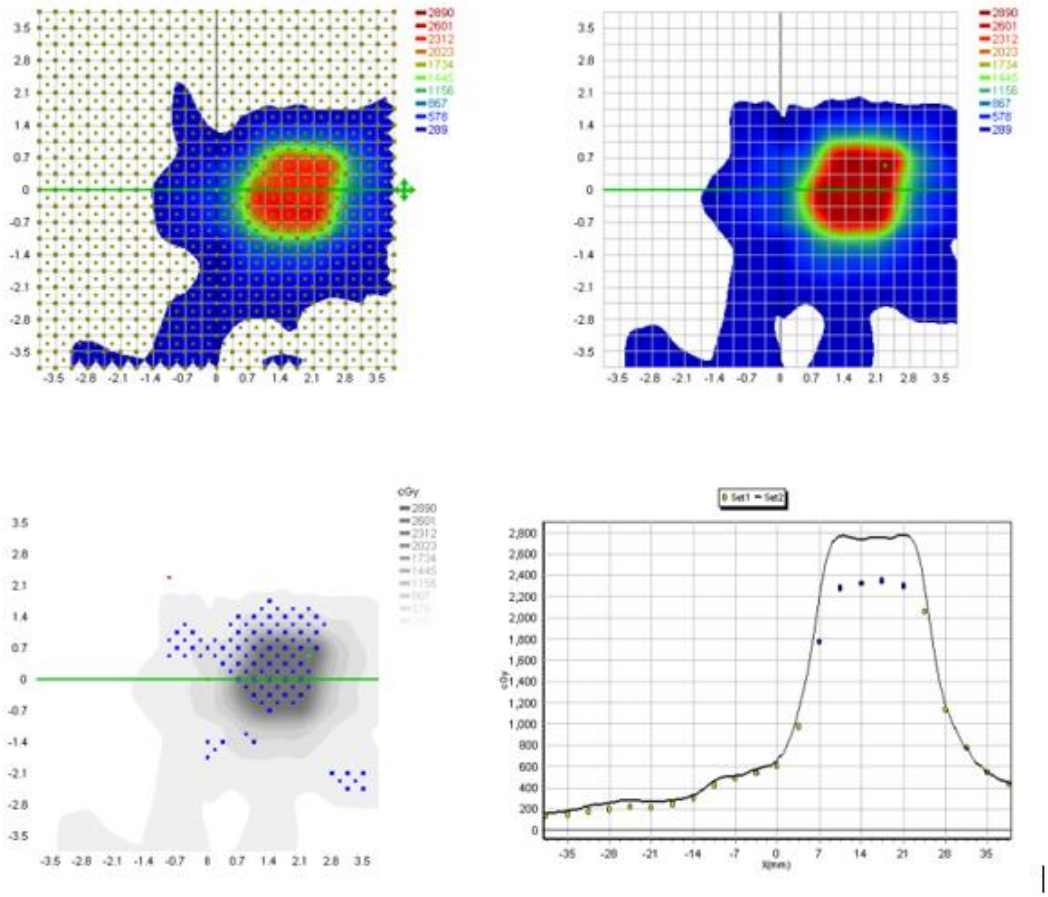

Pass (%)	78.6
Pass	372
Fail	101
Total Points	473

Figure B-13: SRS Mapcheck QA case 41080 original plan

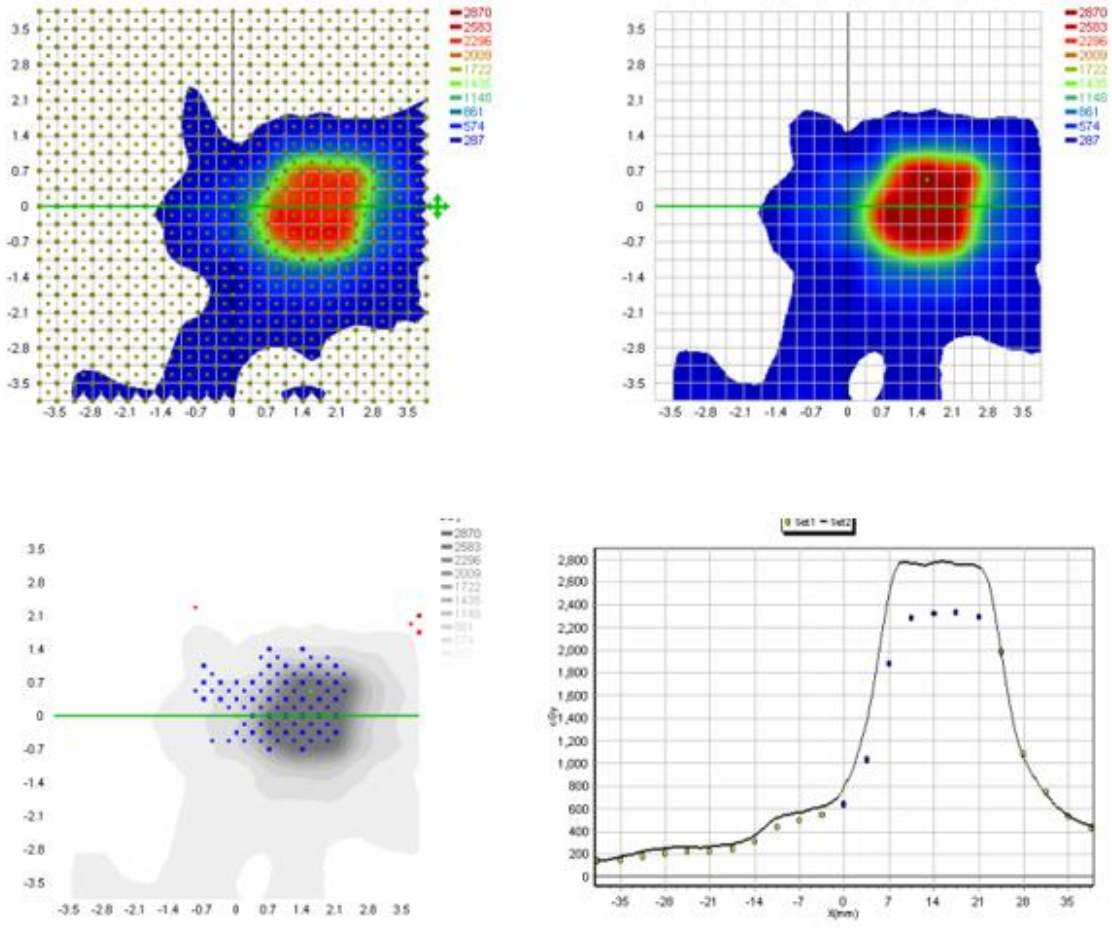

Figure B-14: SRS Mapcheck QA case 41080 AXBe plan

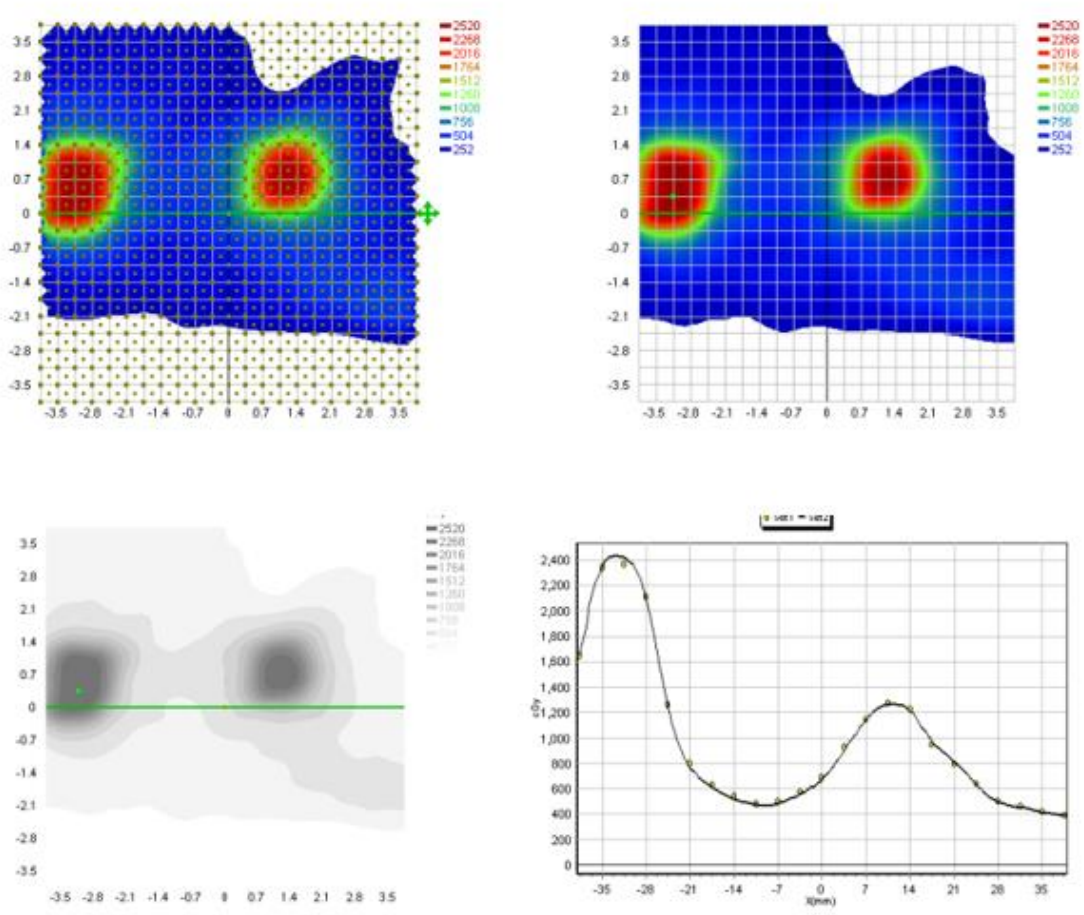

Pass (%)	100.0
Pass	739
Fail	0
Total Points	739

Figure B-15: SRS Mapcheck QA case 17656 original plan

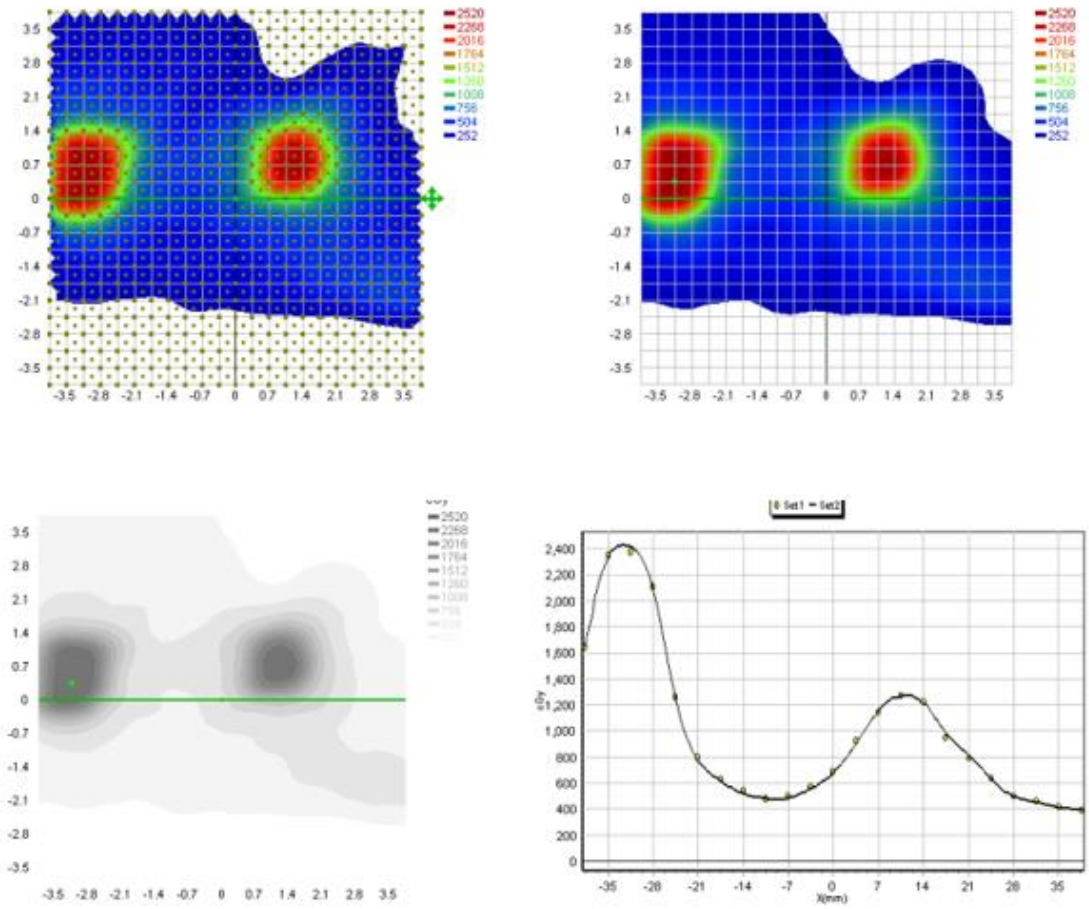

Figure B-16: SRS Mapcheck QA case 17656 AXBe plan

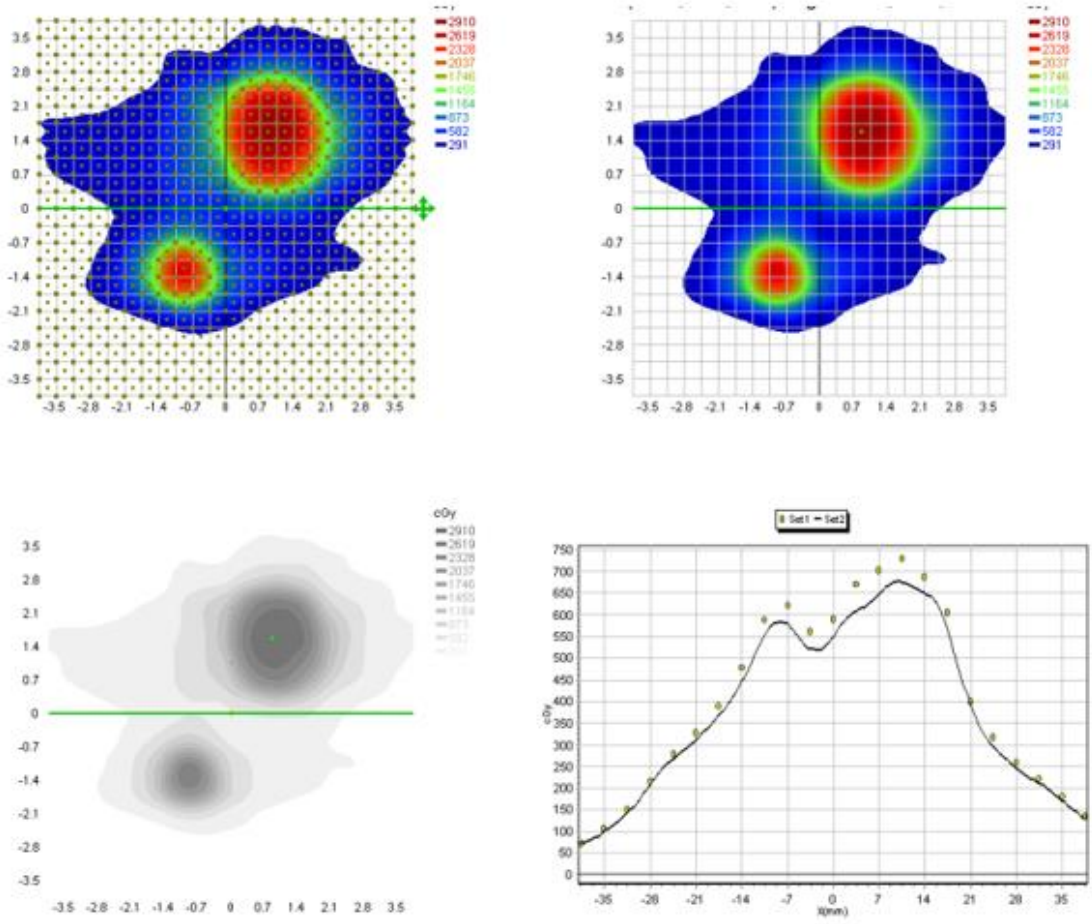

Pass (%)	100.0
Pass	527
Fail	0
Total Points	527

Figure B-17: SRS Mapcheck QA case 88942 original plan

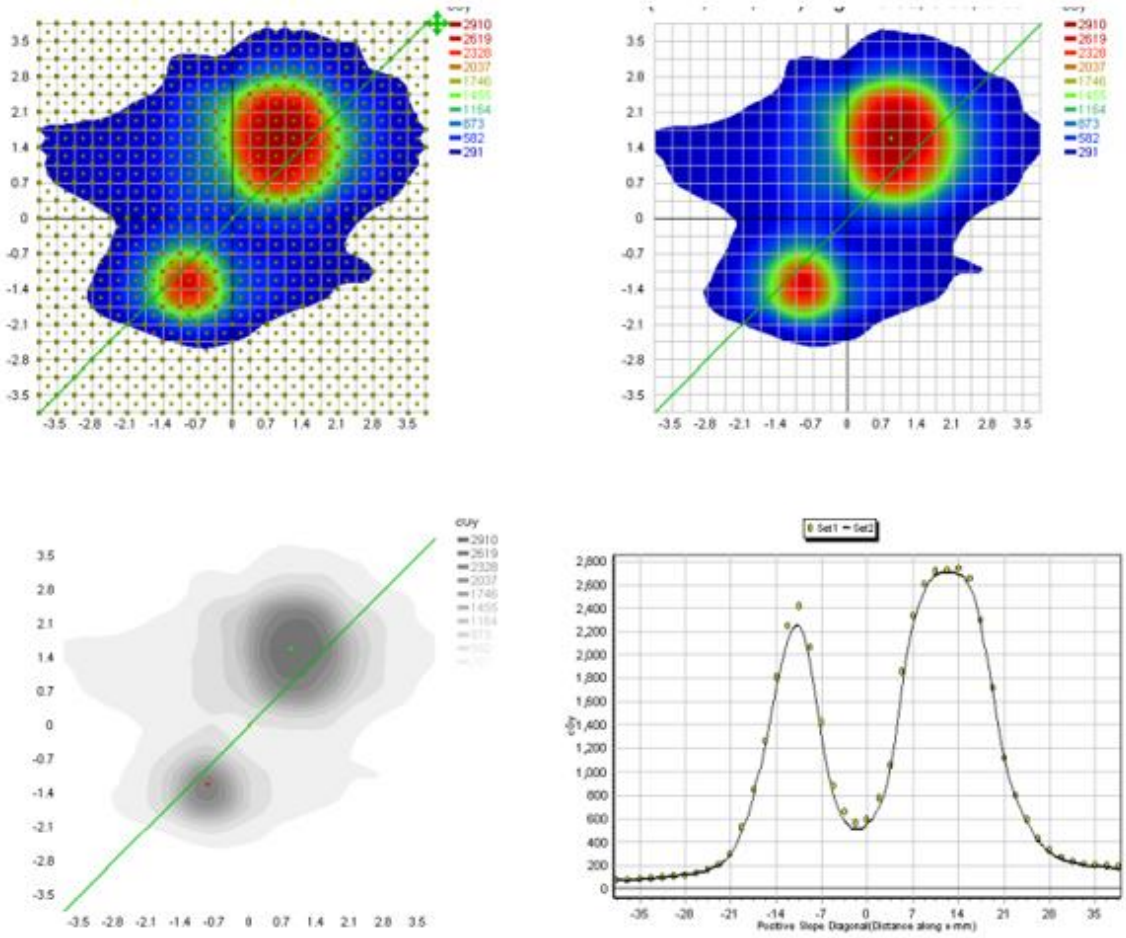

Pass (%)	99.8
Pass	525
Fail	1
Total Points	526

Figure B-18: SRS Mapcheck QA case 88942 AXBe plan

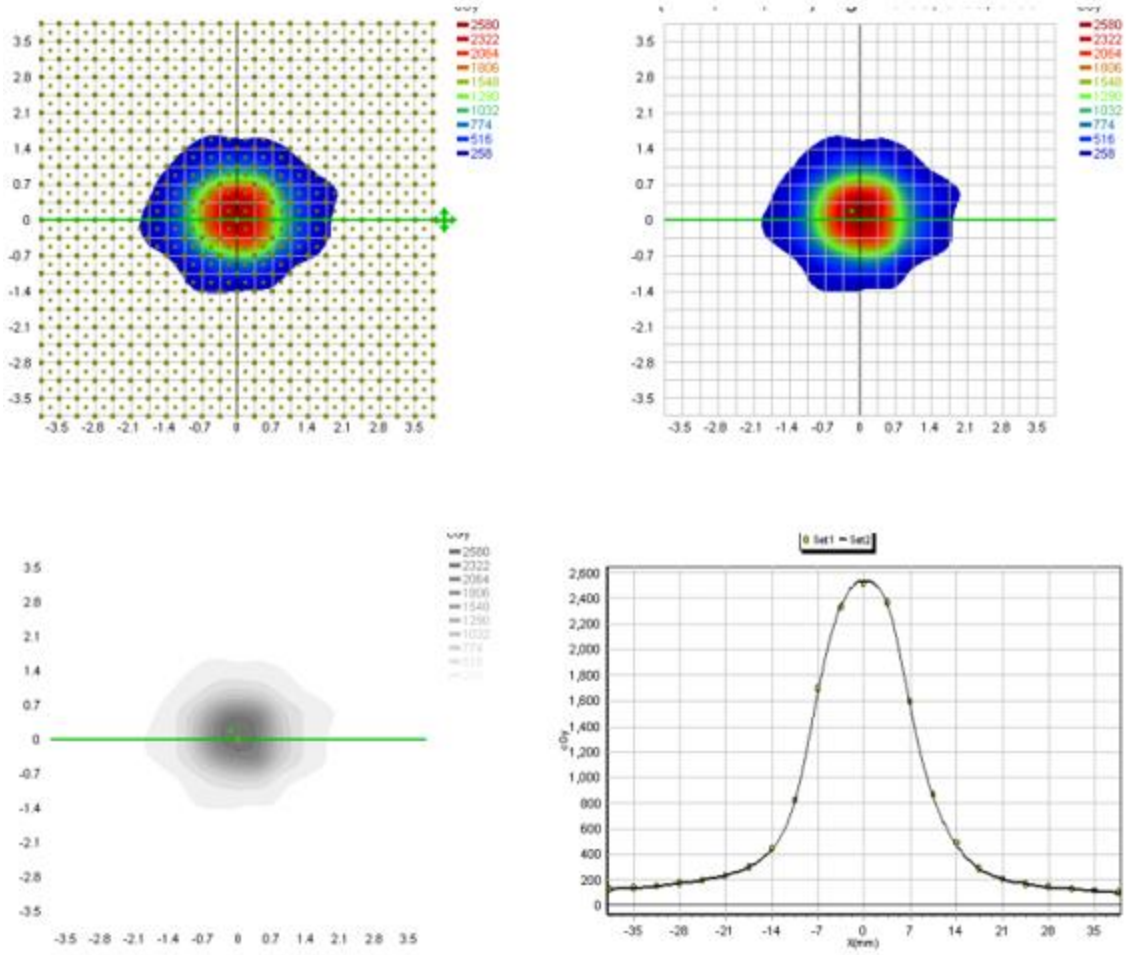

Pass (%)	100.0
Pass	146
Fail	0
Total Points	146

Figure B-19: SRS Mapcheck QA case 38946 original plan

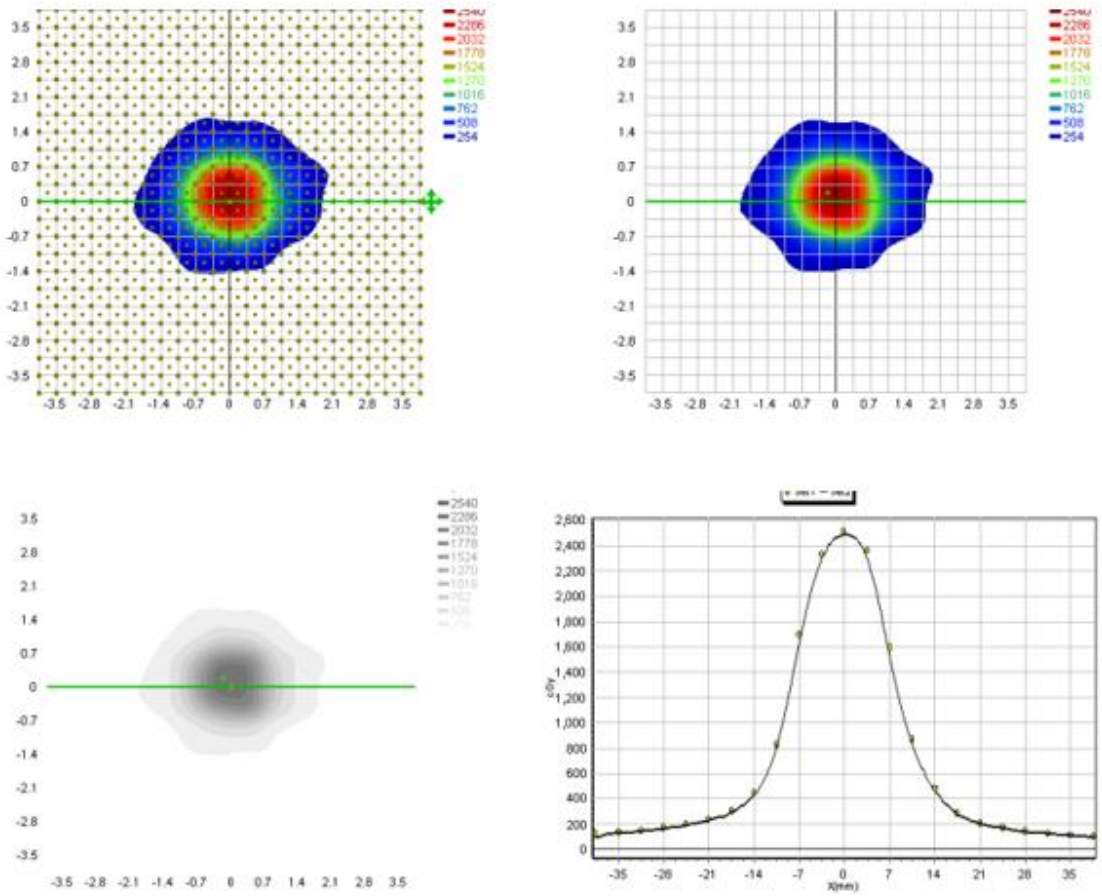

Pass (%)	100.0
Pass	151
Fail	0
Total Points	151

Figure B-20: SRS Mapcheck QA case 38946 AXBe plan

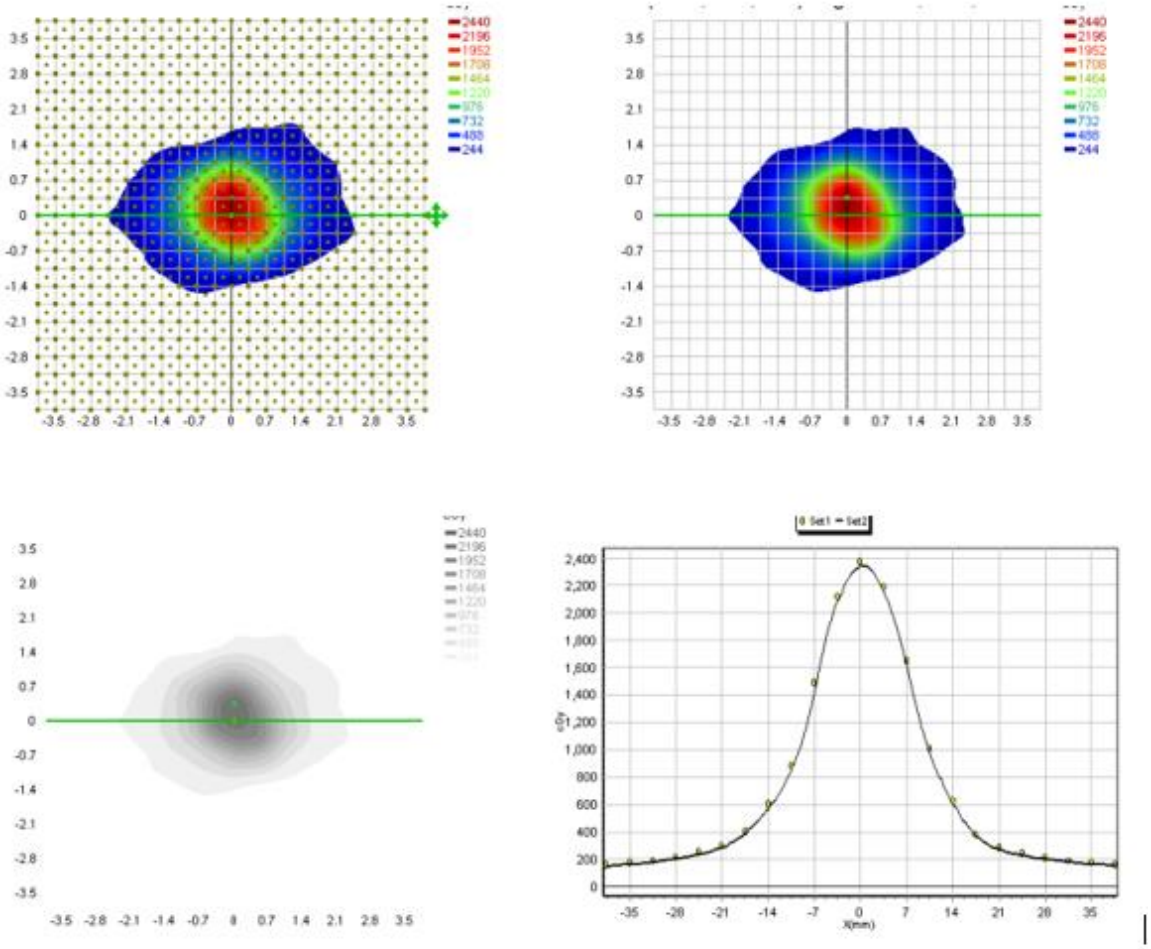

Pass (%)	100.0
Pass	194
Fail	0
Total Points	194

Figure B-21: SRS Mapcheck QA case 59758 original plan

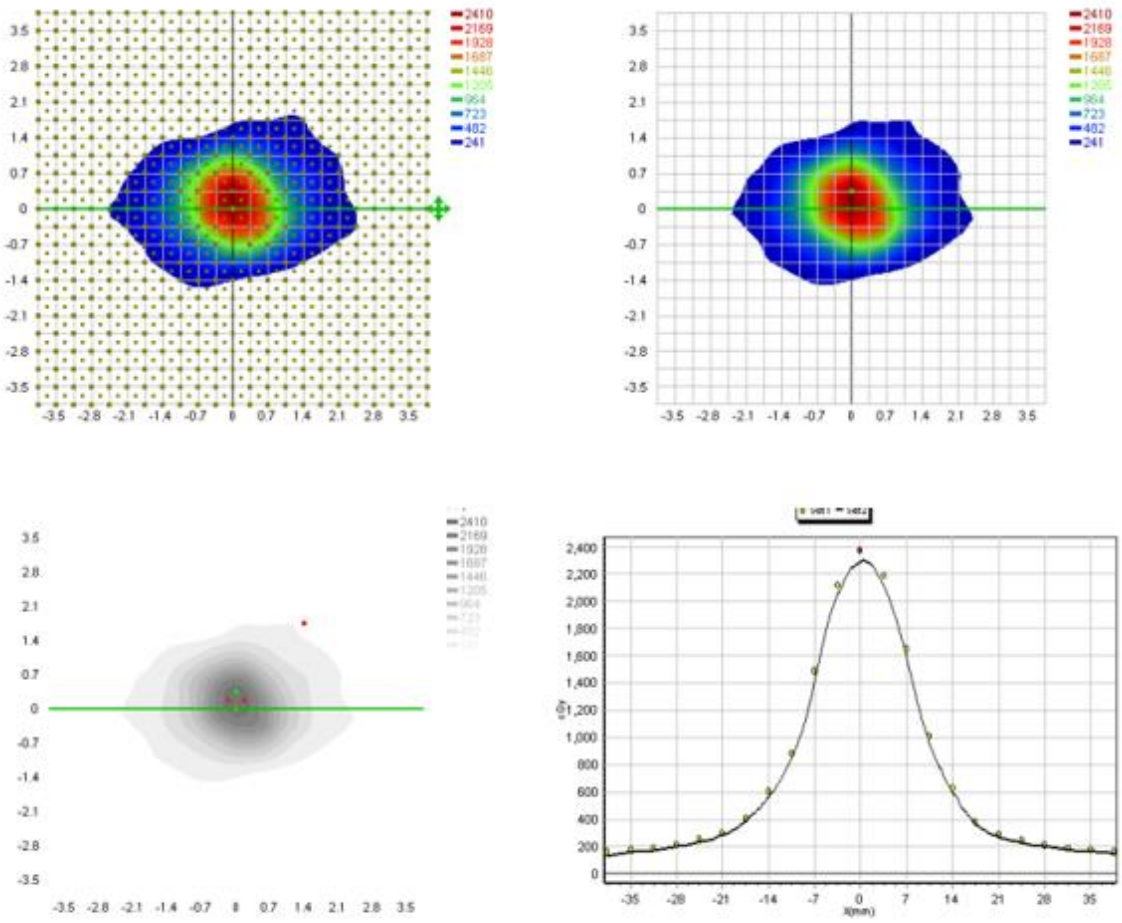

Pass (%)	97.5
Pass	194
Fail	5
Total Points	199

Figure B-22: SRS Mapcheck QA case 59758 AXBe plan

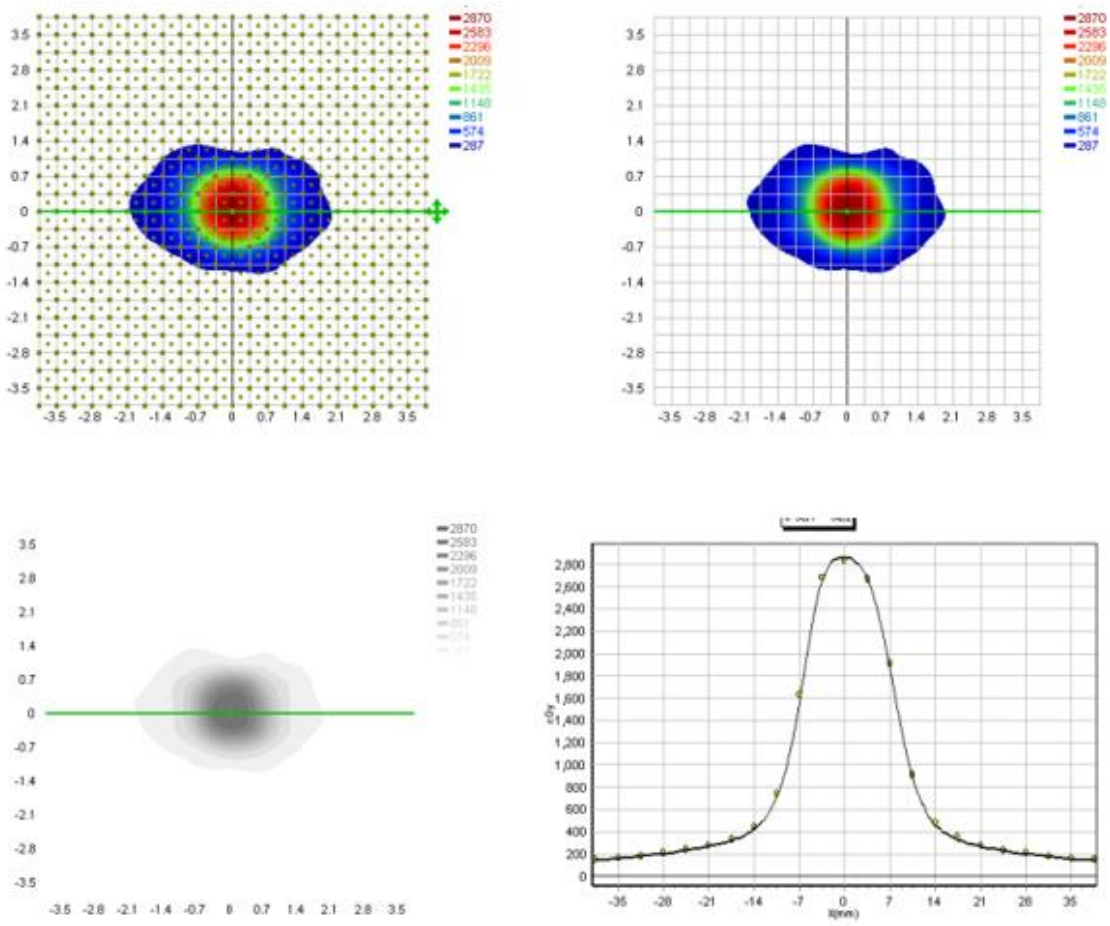

Pass (%)	100.0
Pass	128
Fail	0
Total Points	128

Figure B-23: SRS Mapcheck QA case 20063 original plan

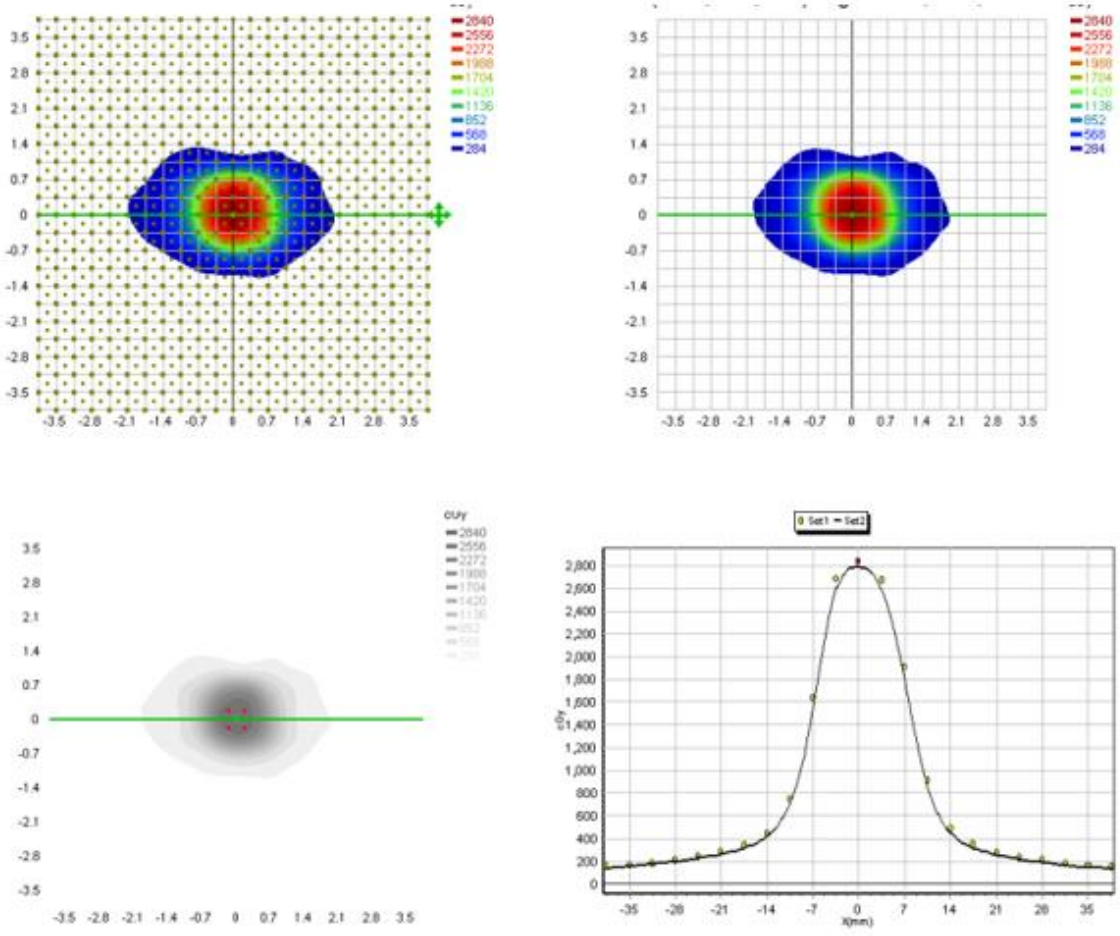

Pass (%)	96.2
Pass	127
Fail	5
Total Points	132

Figure B-24: SRS Mapcheck QA case 20063 AXBe plan

APPENDIX C. PYTHON CODE

```python
import numpy as np
import matplotlib.pyplot as plt
from scipy.interpolate import splev, splrep

# Your data points
x = np.array([8, 6.0, 4.0, 3, 2.5, 2, 1.5, 1.2, 1, 0.8])
y = np.array([1, 1, 1, 1, 1.001, 1.003, 1.008, 1.017, 1.027, 1.043])

# Ensure x is in increasing order
x = x[::-1]
y = y[::-1]

# Perform spline interpolation
tck = splrep(x, y, s=0)

# Generate x values for every 1 mm (0.1 unit) increment
x_mm_increments = np.arange(min(x), max(x) + 0.01, 0.01)
y_mm_increments = splev(x_mm_increments, tck)

# Plotting
plt.plot(x, y, 'o', label='Original data')
plt.plot(x_mm_increments, y_mm_increments, label='Spline interpolation (0.1 mm increments)')
plt.xlabel('X')
plt.ylabel('Y')
plt.legend()
plt.title('Spline Interpolation of Given Data')
plt.show()

# Print table of results
print("Table of Y-values for each 1 mm increment along the X-axis:")
print("X (mm)     Y")
print("--------------------")
for xi, yi in zip(x_mm_increments, y_mm_increments):
    print(f"{xi:.2f}        {yi:.6f}")
```

Figure C-1: Example of the python code used to create data points for the spline interpolations. This example is for the Exradin A16 Micro ion chamber. For each detector, the corresponding x and y values were adjusted to match the field size and output correction factors from Figure 3-1.

REFERENCES

[1] International Atomic Energy Agency. TECHNICAL REPORTS SERIES NO. 483: DOSIMETRY OF SMALL STATIC FIELDS USED IN EXTERNAL BEAM RADIOTHERAPY [Internet]. 2017 [cited 2024 Oct 17]. Available from: https://www-pub.iaea.org/MTCD/Publications/PDF/D483_web.pdf

[2] Ma CMC, Chetty IJ, Deng J, Faddegon B, Jiang SB, Li J, et al. Beam modeling and beam model commissioning for Monte Carlo dose calculation-based radiation therapy treatment planning: Report of AAPM Task Group 157. Medical Physics [Internet]. 2019 Nov 19 [cited 2024 Oct 17];47(1). Available from: https://aapm.onlinelibrary.wiley.com/doi/pdf/10.1002/mp.13898

[3] Failla G, Wareing T, Archambault Y, Thompson S. Acuros_ClinicalPerspectives_RAD10156A_April2015.pdf [Internet]. varian.widen.net. [cited 2024 Oct 17]. Available from: https://varian.widen.net/view/pdf/xo1pmzdzjb/Acuros_ClinicalPerspectives_RAD10156A_April2015.pdf?u=wefire

[4] Zavan R, McGeachy P, Madamesila J, Villarreal-Barajas JE, Khan R. Verification of Acuros XB dose algorithm using 3D printed low-density phantoms for clinical photon beams. Journal of Applied Clinical Medical Physics [Internet]. 2018 May [cited 2024 Oct 17];19(3):32–43. Available from: https://oce.ovid.com/article/02003428-201805000-00008/HTML

[5] Chetvertkov M, Monroe JI, Boparai J, Solberg TD, Pafundi DH, Ruo RL, et al. NRG Oncology Survey on Practice and Technology Use in SRT and SBRT Delivery. Frontiers in Oncology [Internet]. 2020 Nov 27 [cited 2024 Oct 17];10. Available from: https://pmc.ncbi.nlm.nih.gov/articles/PMC7729187/

[6] Followill DS, Kry SF, Qin L, Leif JL, Molineu A, Alvarez P, et al. The Radiological Physics Center's Standard Dataset for Small Field Size Output Factors. Journal of Applied Clinical Medical Physics [Internet]. 2012 Aug 8 [cited 2023 May 27];13(5):282–9. Available from: https://pmc.ncbi.nlm.nih.gov/articles/PMC5718235/

[7] Lechner W, Wesolowska P, G. Azangwe, Mehenna Arib, Gabriel V, Luo Suming, et al. A multinational audit of small field output factors calculated by treatment planning systems used in radiotherapy. Physics and Imaging in Radiation Oncology [Internet]. 2018 Jan 1 [cited 2024 Oct 17];5:58–63. Available from: https://www.sciencedirect.com/science/article/pii/S2405631617300489?via%3Dihub

[8] Dufreneix S, Bellec J, Josset S, Viellevigne L. Field Output Factors for Small Fields: A Large Multicentre Study [Internet]. ClinicalKey. Elsevier; 2021 [cited 2024 Oct 17]. Available from: https://www.clinicalkey.com/#!/content/playContent/1-s2.0-S1120179721000028?returnurl=null&referrer=null

[9] Wu NG. Extending the Eclipse AcurosXB output factor table for small field radiosurgery. Journal of Applied Clinical Medical Physics [Internet]. 2022 Dec 31 [cited 2024 Oct 17];24(1). Available from: https://www.ncbi.nlm.nih.gov/pmc/articles/PMC9859982/

[10] Smith CL, Montesari A, Oliver CP, Butler DJ. Evaluation of the IAEA-TRS 483 protocol for the dosimetry of small fields (square and stereotactic cones) using multiple detectors [Internet]. Ovid. 2020 [cited 2024 Oct 17]. Available from: https://oce.ovid.com/article/02003428-202002000-00013/HTML

[11] Eclipse | Varian [Internet]. www.varian.com. [cited 2024 Oct 17]. Available from: https://www.varian.com/products/radiotherapy/treatment-planning/eclipse

[12] Little A. How does Eclipse determine output for fields smaller than the smallest measured output factor? 2024.

[13] Zidar Casar B, Gershkevitsh E, Mendez I, Jurkovi S, Huq M. A novel method for the determination of field output factors and output correction factors for small static fields for six diodes and a microdiamond detector in megavoltage photon beams. Medical Physics. 2018 Dec 24;46(2).

[14] EDGE DetectorTM - Sun Nuclear [Internet]. www.sunnuclear.com. Available from: https://www.sunnuclear.com/products/edge-detector

[15] RAZOR DETECTOR USER'S GUIDE RAZOR Detector Instructructions for Use. IBA; 2023 Oct.

[16] Partanen M, Niemelä J, Ojala J, Keyriläinen J, Kapanen M. Properties of IBA Razor Nano Chamber in small-field radiation therapy using 6 MV FF, 6 MV FFF, and 10 MV FFF photon beams. Acta Oncologica [Internet]. 2021 Oct 1 [cited 2024 Oct 17];60(11):1419–24. Available from: https://doi.org/10.1080/0284186X.2021.1979644

[17] Das IJ, Dogan SK, Gopalakrishnan M, Ding GX, Longo M, Franscescon P. Validity of equivalent square field concept in small field dosimetry. Medical Physics [Internet]. 2022 Mar 16 [cited 2024 Oct 17];49(6):4043–55. Available from: https://wileyonlinelibrary.com/journal/mp

[18] Blue Phantom2 User's Guide [Internet]. IBA Dosimetry; 2021 Jun [cited 2024 Oct 17]. Available from: www.iba-dosimetry.com